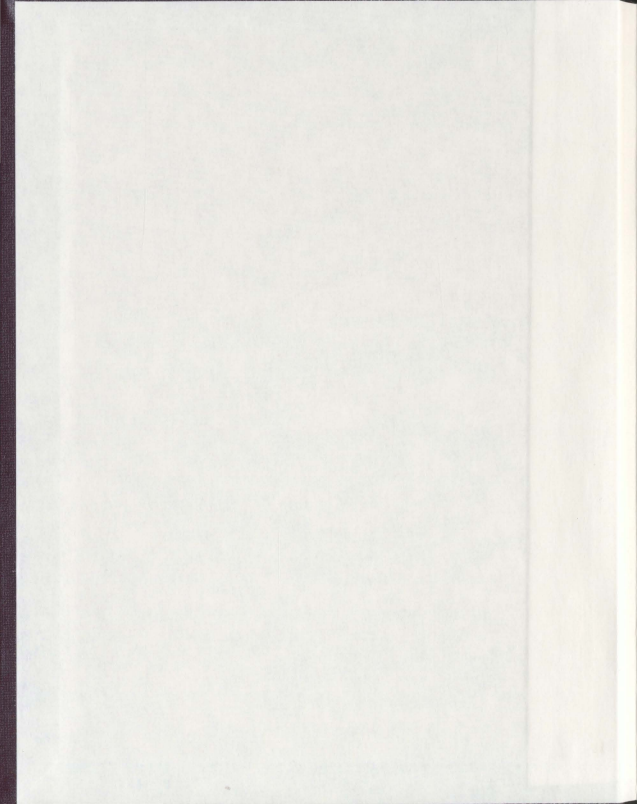


SIMULATING VEGETATION CHANGE IN THE TORNGAT
MOUNTAINS, LABRADOR USING A CELLULAR
AUTOMATA-MARKOV CHAIN MODEL

MICHAEL UPSHALL



SIMULATING VEGETATION CHANGE IN THE TORNGAT MOUNTAINS,
LABRADOR USING A CELLULAR AUTOMATA-MARKOV CHAIN MODEL

BY

©MICHAEL UPSHALL

A thesis submitted to the
School of Graduate Studies
in partial fulfillment of the
requirements for the degree of
Master of Science

Department of Geography
Memorial University of Newfoundland

September 2011

St. John's

Newfoundland and Labrador

ABSTRACT

Changes in vegetation distribution due to climate change are a concern in alpine tundra ecosystems. Past vegetation change was assessed and a cellular automata-Markov (CA-Markov) model was used to predict future land cover scenarios in the Torngat Mountains National Park Reserve (Labrador, Canada). Post-classification image comparison was applied to classified, multi-temporal satellite imagery to detect changes in vegetation patterns since 1985. Deciduous shrubs (typically less than 3m in height) increased in areal coverage whereas heath (low-growing, woody vegetation) experienced a decrease in coverage. Transition matrices were developed from these observed changes, and were used in the Markov chain component of the model. Topographic variables were classified, and used as prior information to calculate Bayesian probabilities (B_{Prob}). The B_{Prob} 's describe suitable areas of growth based on known patterns and were used as a suitability map in the cellular automata component of the model. The CA-Markov model was initially used to predict a known vegetation pattern for 2008, using classified imagery from 1985 and 2001. The model predicted the 2008 land cover with 70.7% accuracy and data, recorded in 2008, was used to predict scenarios for 2018, 2028, and 2038. Results of the CA-Markov simulations show that deciduous shrubs will increase in area by 7.7% but heath will decrease by 14.4%. The results indicate that deciduous shrubs have a tendency to move into higher elevations over an extended period of time.

ACKNOWLEDGEMENTS

This thesis would not have been possible without contributions from many people. First and foremost, I would like to thank my supervisor, Dr. Alvin Simms for his guidance and encouragement throughout this research. I also thank Dr. Elizabeth Simms for many helpful suggestions and assistance with satellite image analysis. I am grateful to Dr. Luise Hermanutz for her leadership and support in the field. She provided me with the resources I needed to complete my field work in an unexpectedly shortened field season. My field work would not have been possible without the assistance of Daniel Myers, Sarah Chan, Hasan Tretina and Dr. Darroch Whitaker, who each spent significant time visiting field sites and recording data with me. I also thank all other members of the Labrador Highlands Research Group for making field camp an enjoyable place stay. I would also like to show my gratitude to Heather Morrison for her help with image analysis and providing feedback on my writing. Finally, I would like to thank Zack Bartlett for the discussions concerning every aspect of this research and the many laughs we shared during the long days in the office.

CONTENTS

Abstract	ii
Acknowledgements	III
Contents	IV
List Of Tables	VII
List Of Figures	IX
List Of Equations	XI
List Of Abbreviations	XII
1. Introduction	1
1.1 Rationale	1
1.2 Purpose	3
1.3 Research Objectives	3
1.4 Study Area	4
1.5 Context Of Research	6
2. Literature Review	9
2.1 Topographic Variables	9
2.2 Change Detection Analysis	12
2.2.1 Image Differencing	12
2.2.2 Post-Classification Comparison	13
2.3 Bayesian Methods	14
2.4 Cellular Automata, Markov Chain Analysis	17
2.4.1 Cellular Automata	17

2.4.2 Markov Chain Analysis	20
2.4.3 Cellular Automata Markov Chain Analysis	23
2.5 Literature Review Summary	24
3. Data Sources	25
3.1 Field Data	25
3.2 Satellite Imagery	30
3.3 Image Classification	31
3.3.1 1985 Classification	32
3.3.2 Indicator Kriging	37
3.3.3 1992, 2001, And 2008 Classifications	45
3.4 Topographic Variables	51
3.4.1 Elevation	51
3.4.2 Aspect	52
3.4.3 Slope	53
3.4.4 Relative Moisture Index	54
3.4.5 Terrain Shape Index	55
3.5 Landscape Description	56
3.6 Climate Data	61
3.7 Summary Of Data	62
4. Preliminary Results	64
4.1 Change Detection	64
4.1.1 Post-Classification Image Comparison	64
4.1.2 Climate Change Assessment	72
4.1.3 Summary Of Change Detection Analysis	78
4.2 Bayesian Probabilities	78
4.2.1 Calculating Bayesian Probabilities	79
4.2.2 Bayesian Probabilities For Change Detection	83
4.2.3 Summary Of Bayesian Analysis	90
5. Cellular Automata Markov Chain Modelling Results	91

5.1 Overview.....	90
5.1.1 CA-Markov Model.....	90
5.1.2 Error Assessment.....	93
5.2 CA Markov Model Development And Accuracy Assessment	95
5.3 Transition Matrices	98
5.3.1 Transition Area Matrices.....	99
5.3.2 Transition Probability Matrices	101
5.4 Cellular Automata Markov Chain Simulations.....	103
5.5 Summary Of Results	112
6. Conclusion	114
6.1 Classified Time Series	114
6.2 Change Detection Analysis.....	115
6.3 Bayesian Probabilities.....	115
6.4 CA-Markov Model Accuracy Assessment	116
6.5 Modelling Future Land Cover Scenarios	117
6.6 Implications.....	120
7. References.....	121
Appendix A: Field Data.....	125

LIST OF TABLES

Table 3.1 Land cover classifications used in this project (Typical plots for each land cover are shown on the right).	29
Table 3.2 Vegetation accuracy for original 1985 classification.....	33
Table 3.3 Vegetation accuracy for purified 1985 classification	37
Table 3.4 Vegetation accuracy for the interpolated 1985 classification	41
Table 3.5 Summary statistics of errors for the interpolated surface.	42
Table 3.6 Vegetation accuracy for the 1992 classification	45
Table 3.7 Vegetation accuracy for the 2001 classification	46
Table 3.8 Vegetation accuracy for the 2008 classification	46
Table 3.9 Kappa Index of Agreement (KIA) values for all classifications.....	46
Table 3.10 Classification scheme for elevation.	52
Table 3.11 Classification scheme for aspect based on equal interval divisions.	53
Table 3.12 Classification scheme for slope adapted from (Dobos <i>et al.</i> , 2005).....	54
Table 3.13 Classification scheme for RMI adapted from Young, (2006).....	55
Table 3.14 Classification scheme for TSI adapted from (Zimmermann, 2001).	56
Table 3.15 Elevation statistics for each land cover class.	57
Table 4.1 Proportion of land cover class present in 2008.....	65
Table 4.2 Prior probabilities for each classified image (%).	80
Table 5.1 Description of Kappa statistics for assessing the accuracy of simulated land cover layers (Pontius Jr., 2000).....	95
Table 5.2 Cross-classification table for the original 2008 classification and the 2008 simulation.....	98
Table 5.3 Transition area matrix for the 2018 projection (%).	100
Table 5.4 Transition area matrix for the 2028 projection (%).	100
Table 5.5 Transition area matrix for the 2038 projection (%).	100
Table 5.6 Transition probability matrix for the 2018 projection	102

Table 5.7 Transition probability matrix for the 2028 projection	102
Table 5.8 Transition probability matrix for the 2038 projection	102

LIST OF FIGURES

Figure 1.1 Predicted annual temperature change for North America between 1980-1999 and 2080-2099.	2
Figure 1.2 Study area extent, Tornгат Mountains National Park Reserve.....	5
Figure 1.3 Relief map for study region, Tornгат Mountains.	7
Figure 2.1. A three-by-three Moore neighborhood and a Von Neumann neighborhood...19	
Figure 3.1. Field locations visited between August 5 th and August 14 th , 2008.	26
Figure 3.2 Plot scheme for arctic tundra regions..	27
Figure 3.3 Original classification for 1985.	34
Figure 3.4 Purified classification for 1985.....	36
Figure 3.5. Probability of finding HG in the problem region of the 1985 classification ...39	
Figure 3.6. Maximum likelihood classification of 1985 Landsat MSS image.	40
Figure 3.7 Histogram showing frequency of errors from kriged model.	42
Figure 3.8 Overestimated and underestimated errors	44
Figure 3.9 Maximum likelihood classification for 1992 Landsat 5 TM image.	48
Figure 3.10 Maximum likelihood classification for 2001 Landsat 7 TM image	49
Figure 3.11 Maximum likelihood classification for 2008 SPOT image	50
Figure 3.12 Histogram of elevation per land class.	57
Figure 3.13 Histogram showing distribution of aspect per land class.	58
Figure 3.14 Histogram showing the distribution of slope per land class.....	59
Figure 3.15 Histogram showing the distribution of RMI per land class.....	60
Figure 3.16 Histogram showing the distribution of TSI per land class.	61
Figure 4.1 Total area of each land cover class for classification in the historical time series.	66
Figure 4.2 Total area for DSH class over the time series.	66
Figure 4.3 Total area gained and lost between 1985 and 2008 for each land cover class. 68	
Figure 4.4 Net change for each land cover class between 1985 and 2008.	68

Figure 4.5 Areas of gains and losses of HG class between 1985 and 2008.....	69
Figure 4.6 Areas of gains and losses in DSH between 1985 and 2008	71
Figure 4.7 Theil-Sen median trend in temperature.	73
Figure 4.8 Fitted seasonal curves for 1985-1991 and 2001-2007.....	74
Figure 4.9 Amplitude 0	76
Figure 4.10 Amplitude 1	76
Figure 4.11 Trend in average mean temperature compared to change in area of vegetation class.....	77
Figure 4.12 Bayesian probability map for DSH in 2008.	83
Figure 4.13 Profile of Bayesian conditional probabilities (%).	83
Figure 4.14 Difference in Bayesian probabilities for DSH between 1985 and 2008.....	86
Figure 4.15 Difference in Bayesian probabilities for HG between 1985 and 2008.....	88
Figure 4.16 Difference in Bayesian probabilities for RCK between 1985 and 2008.	89
Figure 5.1 Original 2008 classification and the simulated 2008 classification	97
Figure 5.2 Projected land cover distributions using CA-Markov chain model.	104
Figure 5.3 Area of each land cover class as represented by the classified imagery and model projections.....	105
Figure 5.4 Area of DSH from the classified imagery and the model projections.....	105
Figure 5.5 Differences in area as observed from classified imagery and projected by the CA-Markov model.	106
Figure 5.6 Transitions between classes for the 2038 CA-Markov projection.	107
Figure 5.7 Gains and losses in RCK for the 2038 CA-Markov chain projection	108
Figure 5.8 Gains and losses in HG for the 2038 CA Markov projection.....	110
Figure 5.9 Gains and losses in DSH for the 2038 CA-Markov projection	111

LIST OF EQUATIONS

Equation 2.1 Image Differencing.....	12
Equation 2.2. Conditional Probability	15
Equation 2.3. Conditional Probability of Multiple Events.	15
Equation 3.1 Relative Moisture Index	54
Equation 3.2 Terrain Shape Index.....	55
Equation 4.1 Prior probability.....	79
Equation 4.2 Bayesian probability.....	79
Equation 4.3 Probability of finding unique combinations of topographic variables	80
Equation 4.4 Image differencing.....	84

LIST OF ABBREVIATIONS

- B_{Prob}: Bayesian Probabilities
CA: Cellular Automata
CA-Markov: Cellular Automata Markov Chain
CiCAT: Climate Change Impacts on Canadian Arctic Tundra
DEM: Digital Elevation Model
DSH: Deciduous Shrub
HG: Heath/Grass
IPY: International Polar Year
KIA: Kappa Index of Agreement
LCM: Land Change Modeler
LHRG: Labrador Highlands Research Group
MC: Markov Chain
RCK: Rock
RMI: Relative Moisture Index
TM: Thematic Mapper
TSI: Topographic Shape Index

LIST OF APPENDICES

Appendix A: Field Data.....	126
-----------------------------	-----

1. INTRODUCTION

1.1 Rationale

Recent studies have shown there has been a warming trend in the earth's climate during the past one hundred years and that temperatures are increasing at a faster rate than ever before (ACIA, 2005; IPCC, 2007). General circulation models predict future climate scenarios and are being developed with increased scrutiny in an attempt to reduce model errors that may have been overlooked in the past. This is done to try to remove some of the uncertainty associated with predicting how climate may change. These models (Figure 1.1) have shown that the greatest amounts of warming and increases in precipitation will occur in high latitude ecosystems (ACIA, 2005; IPCC, 2007). Arctic regions may experience a warming up to 5°C while southern regions will warm by 2 to 3°C. These changes may impact ecosystems throughout the world with increased intensity and frequency of storms as well as shifts in plant and animal geographic extent (IPCC, 2007). Cannone *et al.* (2007) determined that vegetation in the European Alps experienced more growth with increased temperatures between 1950 and 2003. They found that alpine ecosystems are in danger of experiencing changes in vegetation distribution and extent, if the temperature increase continues. It has also been shown that climate is often the major limiting factor when it comes to vegetation growth (Korner and Paulsen, 2004; Pauli *et al.*, 1996). This suggests that increases in temperature correspond with increased species diversity at high elevations. Shifts in species habitat could therefore be more pronounced in the alpine regions than at lower elevations.

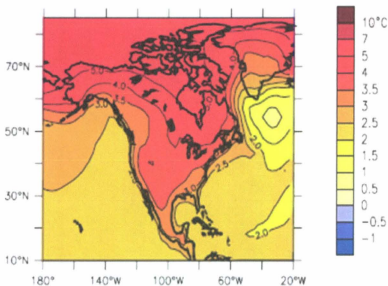


Figure 1.1 Predicted annual temperature change for North America between 1980-1999 and 2080-2099, averaged over 21 models. Source: Intergovernmental Panel on Climate Change (IPCC), 2007.

Understanding the relationship between vegetation, topographic and climatic conditions are factors in determining how vegetation will react to changing climate. Developing spatial models is one way of investigating these relationships and understanding how vegetation distributions will advance and move upslope in an alpine environment (Guisan and Zimmermann, 2000).

1.2 Purpose

The earth's future climate can be understood by assessing the response of existing ecosystems to change in temperature. The study site, located at 58° 38.5' N, 63° 22.5' W, is within the newly established Tornгат Mountains National Park Reserve in Labrador, Canada. Land management, park zoning and continued monitoring are all issues that will likely be addressed in the future and the results of this research could potentially be used in supporting these management decisions. Predictions of vegetation scenarios will provide some insight to the impending stresses exerted on this fragile alpine ecosystem. The methodology used in this research could also be expanded to incorporate larger areas of the park so that vegetation dynamics can be understood over extended regions. The research will encourage park managers to continue data collection year round to develop more complete and accurate data sets. Accurate data are the key to attaining greater certainty in predictive models and a better understanding of alpine vegetation dynamics.

1.3 Research Objectives

The main objective for this research project is to develop a predictive model that will incorporate current topographic conditions as well as observed vegetation change over time to determine the future spatial distribution of vegetation in the Tornгат Mountains, Labrador. To achieve this objective, a series of sub-objectives will be addressed:

1. Generate a time series of classified satellite imagery.
2. Determine the quantity and location of vegetation change at the study site.
3. Develop a set of suitability maps for land cover change and Bayesian probability methods.

4. Predict current vegetation patterns in the Torngat Mountains using historic satellite data to assess model accuracy.

1.4 Study Area

Regions in far northern latitudes are expected to be some of the most affected areas on Earth due to climate change. Several projected climate scenarios suggest that the high latitude regions of the world could warm by as much as 7.5°C by 2099 (IPCC, 2007). As a result, impacts on vegetation will be greatest in the north. Vegetation changes are becoming more evident in the landscape and modeling these changes is important to understand the impact that climate change is having on high latitude regions of the world.

Research was conducted in the Torngat Mountains National Park Reserve located in the northernmost part of Labrador. Clark (1988; 1991) documents the glacial history of the region that created the fjords that define the landscape. The specific site is located in the southern portion of the park at approximately 58° 38.5' N, 63° 22.5' W, which is east of Nakvak Brook. The study area covers an area of approximately 35 km² and has an elevation range of 840m (Figure 1.2).

The study area is an appropriate region to assess changing vegetation patterns because it has a number of distinct vegetation types in a relatively small area. This is primarily due to the elevation change from the valley floor near Nakvak Brook, to the highest peak located less than 4km to the east. Although the entire region is considered an Arctic Tundra environment, the vegetation at lower elevations is quite different from the vegetation at higher, more exposed, areas. At low elevations, shrubs can reach approximately 2m in height, but get progressively shorter with increasing elevation.

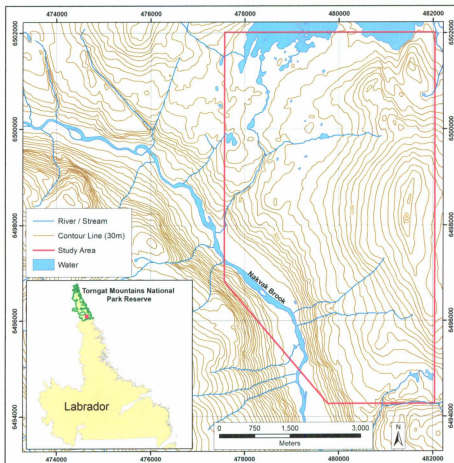


Figure 1.2 Study area extent, Torngat Mountains National Park Reserve

At about 400m, vegetation does not exceed 20-30 cm from the ground. At the highest elevations, frost-shattered rock is the predominant feature and vegetation is almost non-

existent. The changes in elevation throughout the entire region range from 0m to 1155m (Figure 1.3).

There is potential for the vegetation patterns in this region to change with a changing climate. The larger shrubs at lower elevations extend up the side of the valley, indicating the potential for these shrubs to live at higher elevations. Exposure to wind and snow might be the factors that are currently preventing some species from becoming established at the 400m to 750m elevation range. A warming climate, however, could create more favourable conditions at higher elevations. These conditions make the area a suitable location to investigate how vegetation has changed in the past and if shrubs have potential to move upslope in the future.

1.5 Context of Research

The research project is funded by the International Polar Year (IPY) Climate Change Impacts on Canadian Arctic Tundra (CiCAT) project. This CiCAT project is aimed at assessing past, present and future impacts of climate change on tundra ecosystems in Canada (Henry, 2010). IPY also aims to leave a legacy of research results and infrastructure to be used by future researchers and people in northern communities (Henry, 2010).

This research project is part of the work of the Labrador Highlands Research Group (LHRG) at Memorial University of Newfoundland. The LHRG researches the sensitivity of tundra ecosystems to climate change in highland regions of Newfoundland and Labrador, including the Torngat Mountains. The objectives of the LHRG is to

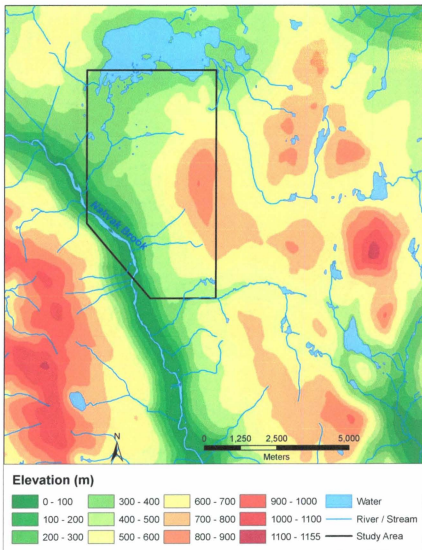


Figure 1.3 Relief map for study region, Torngat Mountains.

understand the evolution of these ecosystems and their relation to local climates and attempts to predict what will happen under future climates (Labrador Highlands Research Group, 2010). This research helps contribute to both the CiCAT and LHRG objectives by investigating the recent history of vegetation change in the region and providing insight into future scenarios.

2. LITERATURE REVIEW

This chapter provides a review of the literature relating to vegetation change in the landscape and how change has been predicted using a cellular automata Markov chain approach. The first section discusses how topographic variables have been used to describe the landscape and how they have been used to illustrate and predict where vegetation will grow. The second section discusses change detection methods applied to satellite imagery. Vegetation change cannot be predicted unless there is evidence that change has occurred in the past. Post-classification comparison and image differencing are presented due to their simple application and effectiveness in detecting change. The third section deals with Bayesian methods and their usage in landscape ecology. The theory behind Bayesian methods will be addressed, including some of the methods in which they have been applied using spatial data. The final section deals with cellular automata Markov chain (CA-Markov) modelling methods. Cellular automata and Markov chain models will be discussed separately as well as how they can be used in conjunction with one another to predict future vegetation patterns.

2.1 Topographic Variables

It has been well documented that basic topographic variables such as elevation, slope and aspect influence vegetation patterns and biodiversity in the landscape (Fu *et al.*, 2004; Ostendorf and Reynolds, 1998; Rezaei and Gilkes, 2005). Moore *et al.* (1991) classified topographic variables into primary and compound classes. The authors considered primary variables to be those related to vegetation patterns, and derived from digital elevation models (DEM). This includes variables such as slope, aspect, elevation, and

curvature which are related to characteristics such as hydrology, solar radiation and soil water content (Moore *et al.*, 1991). Compound variables are substitutes for more complex biophysical processes and include indices for soil moisture, soil properties and terrain shape or position. These positional characteristics can influence vegetation by affecting other variables such as wind and snow exposure, snow accumulation, moisture runoff and accumulation, and soil characteristics (Rezaei and Gilkes, 2005).

Combinations of topographic variables can define where vegetation will grow in the landscape. Elevation can be used to delineate the limits of tree growth as low temperatures at higher altitudes make it difficult for certain types of plants to grow. Similarly, some species would have difficulty growing on steep slopes or on northerly aspects due to insufficient sunlight. These variables are calculated from a DEM and are used to calculate compound variables such as topographic shape or moisture accumulation indices.

Topographic variables have been utilized in recent years for predictive vegetation modelling and to describe and explain vegetation changes in the landscape. The variables used depend on the research objectives and the type of landscape under consideration.

A vegetation model developed by Ostendorf and Reynolds (1998), predicted vegetation patterns in the Arctic by using the inverse relationship between slope and discharge. Discharge was considered a measurement of soil moisture, while slope is inversely related to it. A more detailed methodology is presented by Ostendorf and Reynolds (1998) whereby the authors attain a goodness of fit of 78%, using only two variables in their model. Bennie, *et al.* (2006) also considered two variables when attempting to explain where in the landscape chalk grasslands were changing the most.

Historical data combined with an updated field survey were used to observe change and ANCOVA was used to determine the statistical relationship between the areas of change and the slope and aspect. They were able to determine that flat terrain was much more vulnerable as the amount of change decreased with increasing slope angle. South-facing slopes were found to be the most resistant to change and had more light demanding vegetation while north-facing slopes were less resistant.

Recent studies have focused on how topographic variables affect soil properties and the influence they have on vegetation patterns (Fu *et al.*, 2004; Rezaei and Gilkes, 2005). Several multivariate statistical techniques were used by Fu *et al.* (2004) to assess the relationship that elevation, aspect, slope and slope position had with soil fertility and quality. The results demonstrated that topography is an important factor in explaining the variability in soil properties. It was shown that elevation and aspect had a direct relationship with shrub richness and diversity, while elevation also had a positive relationship with soil organic matter (Fu *et al.*, 2004). Rezaei and Gilkes (2005) examined similar relationships in an alpine rangeland and also found that soil properties exhibit variability based on different topographic conditions. They determined that slope has a particularly strong relationship with soil stability and aspect was directly related to soil nutrients. Primary variables (such as slope, aspect, and elevation) have been shown to have positive relationships with vegetation growth and can be used effectively in analyzing change in the landscape.

2.2 Change Detection Analysis

Documenting past vegetation change is important for understanding present and future conditions. It is difficult to predict future vegetation patterns without an understanding of the topographic and climatic factors that influence those patterns. Earth observing satellite sensors have been recording multispectral satellite imagery since the early 1970s. The affordability of multi-date imagery has made digital change detection, the method of choice when it comes to monitoring urban, rural or natural landscapes. Its popularity has grown due to the increased availability of satellite imagery at a more frequent temporal scale meaning some areas can be monitored on a yearly, monthly or daily basis.

Many change detection methods are being used effectively to detect changing landscapes. Lunetta (1998), Nelson (1983), Singh (1989), Yuan *et al.* (1998) have reviewed digital change detection methods ranging from image differencing to applications of principal components analysis or change vector analysis. The following sections evaluate image differencing and post-classification comparison as two methods that have been used in various applications.

2.2.1 Image Differencing

Image differencing is a common method of change detection analysis which involves subtracting an image band at time t_1 from the same band at time t_2 . This procedure is based on Equation 2.1 (Singh, 1989):

$$Dx_{ij}^k = x_{ij}^k(t_2) - x_{ij}^k(t_1) + C \quad (\text{Equation 2.1 Image Differencing})$$

Where:

x_{ij}^k is the pixel value for band k at the i th row and j th column

t_1 is the earliest date

t_2 is the latest date

C is a constant used to produce positive digital numbers

The output is an image that shows the difference in brightness values between two dates for each pair of bands. A threshold has to be applied to the output in order to identify areas of significant spectral differences. Generally, a threshold is based on standard deviation (SD). Lunetta (1998) states that the lower SD will include greater amounts of the changed pixels and thus a higher potential for errors of commission.

Nelson (1983) evaluated image differencing for delineating gypsy moth defoliation because it was the most widely used method and provided a good comparative index. The SD method of thresholding was used to determine the maximum classification accuracy to within 0.05 SD. The author also found that classification accuracies were comparable to other methods that were tested, making image differencing a useful option. The other techniques were only slightly better than this baseline method, with differences between accuracies being on the order of tenths of a percent.

2.2.2 Post-classification comparison

Another method of change detection is post-classification comparison. This method involves creating classified images through one of a variety of supervised or unsupervised methods. Given classified imagery from two time periods, change maps are created that show differences in vegetation types. This method uses classified satellite imagery, thereby minimizing problems with atmospheric and sensor differences (Singh, 1989). Highly accurate classifications are required in order for change detection to be effective because the joint classification rate is lower than the images from which it is derived. Singh (1989) provides an example of two images with 80% accuracy having only 64%

(80% X 80%) joint accuracy. Post-classification comparison was successfully applied by Weismiller *et al.* (1977), who identified areas of change in coastal zone environments in Texas. Of the four change detection methods they tested, post-classification comparison provided the most reliable results. Mas (1999) demonstrated that the procedure can be applied to vegetation studies if accurate classifications of different land covers are available. Accuracies in excess of 85% were obtained for post-classification analysis which was the best of the change detection methods tested. High change detection accuracies were attributed to the high image classification accuracy. Mas (1999) discusses how this method is less sensitive to radiometric differences and is more appropriate for dealing with a time series of satellite imagery. The nature of the changes is also easily understood because they represent a transition from one type of land cover to another. Post-classification change detection is one of the most effective and intuitive methods of digital change detection if satellite imagery can be accurately classified.

2.3 Bayesian Methods

McCarthy (2007) discusses some of the advantages of using Bayesian methods in the field of ecology. These advantages include:

1. The ability to make predictions about the state of a system.
2. The ability to incorporate prior information into the analysis and thus being able to incorporate multiple sources of information.
3. The ability to be integrated with geographic information systems (GIS) and spatial models for addressing ecological and environmental problems.

As a result, Bayesian methods have become very popular amongst ecologists.

Bayesian analysis can be thought of as incorporating prior knowledge and data into a model to output posterior knowledge. It uses Bayes' rule, which is based on a conditional probability that calculates the probability of "event A" occurring given that "event B" has occurred. Conditional probability has been adapted from Bonham-Carter (1994) and McCarthy (2007) and is given by:

$$P(A|B) = P(A \cap B) / P(B) \quad (\text{Equation 2.2. Conditional Probability})$$

Where:

$P(A|B)$ = the conditional probability of event A, given the presence of event B.

$P(A \cap B)$ = the proportion of total area occupied by events A and B together.

$P(B)$ = the proportion of the total area of occupied by event B.

To assess the probability of event A occurring given the presence of multiple events (B_i and B_{i+1}), the conditional probability can be written as:

$$P(A|B_i \cap B_{i+1}) = P(A \cap B_i \cap B_{i+1}) / P(B_i \cap B_{i+1}) \quad (\text{Equation 2.3 Conditional Probability of Multiple Events})$$

Equation 2.4 is adapted from Bonham-Carter (1994) and can be used with multiple independent events. The output is the probability of finding "event A" given unique combinations of multiple events. The Bayesian conditional probabilities are versatile in that an infinite number of independent events can be used and they can be added or removed at any time to assess a particular variable's impact on the output.

One application of Bayesian methods is presented by Aspinall (1992), who generated a probability model using environmental variables to describe the distribution of red deer in north-east Scotland. This model uses an inductive modelling procedure,

which is based on Bayesian methods, to assess relationships between variables in order to estimate probabilities of occurrence. The procedure was effective in modelling the distribution of red deer and provided error assessments for the model.

Bonham-Carter *et al.* (1988) used Bayesian statistics combined with multiple regression analysis to predict favourable sites for gold exploration in Nova Scotia, Canada. Posterior probabilities were calculated using unique conditions mapping which identified different combinations of the patterns to be modelled. The unique conditions were used to evaluate areas where gold was most likely to occur. The authors acknowledge that several sites with no known gold occurrence were identified by the model. These could be considered sites of potential interest for geologists.

Vaiphasa *et al.* (2006) used Bayesian methods as a post classifier for mangrove mapping in Thailand. They found that integrating soil-related parameters improves the overall accuracy of mangrove maps from 76% to 88%. This is a way of enhancing classified satellite imagery by incorporating additional predictive variables using Bayesian methods.

The above examples demonstrate that Bayesian methods are being considered a final result in terms of probability models. Outputs are given as a probability of occurrence or divided into varying thresholds based on the likelihood of occurrence (Aspinall, 1992; Bonham-Carter *et al.*, 1988). Vaiphasa *et al.* (2006) use the method as a way to refine a classification system; however, the Bayesian process is still the primary method of modelling.

There remains an opportunity for Bayesian statistics to be applied to spatial modelling as a method for defining suitability maps. Bayesian statistics can define the

probability of occurrence of any land cover type based on a set of suitable predictor variables. The probabilities identify areas that are suitable for vegetation growth and can be input into cellular automata (CA) models. CA models require rules that enable and restrict the spatial distribution of specific vegetation. The following section discusses CA-Markov chain models in more detail, while a discussion of incorporating Bayesian statistics into the model is presented in the methodology.

2.4 Cellular automata, Markov chain analysis

Both the cellular automata (CA) model and Markov chain (MC) analysis can be applied as independent models. They also have the ability of being used in conjunction with one another to make predictions about future scenarios. MCs calculate the probability of transitioning from one state to another, over a specified time period. This is used by the CA model to predict future land cover distributions given present suitability conditions. The following sections discuss both CA and MC separately, as well as some examples of how they have been applied elsewhere to vegetation distribution analysis or modelling. The cellular automata Markov chain (CA-Markov) models are discussed, and some examples of how they are used by other researchers is presented.

2.4.1 Cellular automata

In their most common form, CA models are 2-dimensional arrays of regular shaped, square cells. They are not restricted to this form because they can also be comprised of other regular grids of triangles or hexagons, or irregular shaped Voronoi polygons (De Smith *et al.*, 2007; Wolfram, 1983). A CA model can be broken into five separate

components as outlined by De Smith *et al.* (2007). They divide the model into state variables, a spatial framework, neighbourhood structures, transition rules, and time.

State variables refer to the state or value of cells at any particular point in time. In the simplest form of model, the cells are binary although, more complex examples have been developed that incorporate multiple states, such as different land-use classes. These values change as model runs are completed through discrete time steps. The spatial framework is the entire lattice of cells. The 2-D array of cells discussed above would be considered the framework of a CA model.

The third component is the neighbourhood structure, which is the area surrounding each cell of the framework. Neighbourhoods are typically the same for each individual cell; however, there are different forms that can be used. Two common types are the Moore and Von Neumann neighbourhoods (Figure 2.1). The Moore neighbourhood consists of all immediately surrounding cells in an array and can be varying sizes. A three by three Moore neighbourhood incorporates the eight cells adjacent to the centre cell, while a five by five neighbourhood incorporates twenty-four surrounding cells. The Von Neumann only considers the four cardinal neighbours in the analysis (De Smith *et al.* 2007).

The fourth component is the set of transition rules for a CA model. These rules define how each cell of a model will change over time by assessing the states of the cells in the defined neighbourhood, and assigning a value to the cell in question. Most models use simple transition rules to define requirements for change to occur, but recent studies

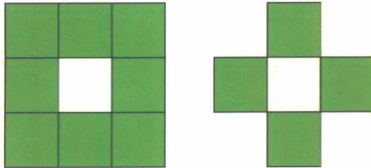


Figure 2.1. A three-by-three Moore neighborhood (left) and a Von Neumann neighborhood (right).

have used probabilistic rules (Colasanti *et al.*, 2007; Lanzer and Pillar, 2002).

The final parameter of a CA model is time, which is defined in discrete steps. At each time interval the transition rules are put into effect and all cells change their state simultaneously. A new state is established and the transition rules are put into effect again for the next time interval (De Smith *et al.*, 2007). These components of a CA model simplify the modelling process and helped make CA a popular method of simulation in a variety of fields.

CA models are used to simulate changing vegetation patterns in the landscape. Colasanti *et al.* (2007) studied high level community processes by utilizing a 2D probabilistic CA model. They used a set of physiologically based rules, derived from a common system of plant functional types, to model individual plant behaviour. The model is based on the plants growth ability, survival ability, and reproductive capabilities and the rules were developed from accepted plant population models.

Lanzer and Pillar (2002) used a set of probabilistic rules, generated from empirical data, to predict land cover as being one of nine classes. They argue that their CA model does not reach a stable final state that would be found with a Markov model. They used several runs of the model to define a range of potential outcomes. Their results indicate that the CA model worked as well as an MC model, which was also used on the same dataset. The research reviewed here are two examples of how CA models have been implemented to model vegetation systems.

2.4.2 Markov chain analysis

Markov chain (MC) models have frequently been used in vegetation studies (Balzter, 2000; Benabdellah *et al.*, 2003; Isagi and Nakagoshi, 1990; Lippe *et al.*, 1985; Pueyo and Begueria, 2007; Usher, 1981). A MC is defined as a stochastic process that fulfills the Markov property (Balzter, 2000). The Markov property states that future conditions do not depend on past conditions. Thus, a MC depends only upon the present state of a system. These models also rely on the assumption that vegetation succession is an orderly process and that probabilities for the transition between different states can be determined (Usher, 1981). Other assumptions include time homogeneity and spatial independence, which implies, changes in one particular location will have no effect on nearby locations (Balzter, 2000). This means that spatial autocorrelation is not accounted for in MC analysis. A Markov chain represents a system of varying states that, over time, make transitions from one state to another.

The MC models require discrete classes as input. Thus when using multi-temporal satellite imagery, a classified image is appropriate. Differences in land cover classes

between images, are used to generate transition probabilities that give the likelihood of a particular class changing. Multiple images allow transition probabilities to be generated for different time periods, which can be compared to determine whether rates of change are increasing or decreasing. It also eliminates the assumption of time homogeneity because a series of models can be constructed to show variation over time (Pueyo and Begueria, 2007).

A distinct advantage of the Markov model is that it can generate reliable predictions of future vegetation states without having to know or understand, all of the underlying processes that create a very complex ecosystem (Balzter, 2000). The result is that the mechanisms of succession are not well understood, even though accurate predictions can be made (Usher, 1981). Obtaining satellite imagery is a much more cost efficient method of observing the Earth than collecting field data on a long term basis. Field work is still required for ground truthing purposes but less time and money is expended investigating underlying processes in the landscape.

Balzter (2000) analyzed twenty-two applications of Markov models that examined grassland communities for various in Europe. Inconsistent results were found in this study because of disturbances that altered ecological factors and generated unpredictable changes in the vegetation. Suggested solutions include the generation of a Hidden Markov model to account for climate variation, and the development of separate transition matrices for shorter time periods to justify time homogeneity (Balzter, 2000). If spatial autocorrelation is present in the data then a spatio-temporal Markov chain might be more appropriate. This type of model requires many more parameters as input thus, the advantage of a simple Markov model, is no longer applicable.

Benabdellah *et al.* (2003) used Markov models to generate predictions of forest succession for their study site in Germany. They generated a time homogeneous Markov model on the assumption that, environmental conditions remain constant. They also generated a time inhomogeneous model for regions that were highly polluted by SO₂. This enabled calculations of transition matrices before and after SO₂ pollution damaged the vegetation. The inhomogeneous model is a way to incorporate disturbance into the analysis. The authors found that the Markov models could be useful for management decisions, but acknowledge that accuracy was only evaluated qualitatively. They claim that a quantitative assessment should be performed on the results to determine the accuracy of the model.

Pueyo and Begueria (2007) predicted secondary vegetation succession after farm abandonment in the Central Spanish Pyrenees. They used a multivariate logistic regression from spatially distributed variables to improve transition probabilities used by the Markov model. This is a way of incorporating abiotic factors into the Markov analysis. They found this method was successful in modelling spatial and temporal patterns of secondary succession. They also identified temperature gradient with elevation, and potential solar radiation, as the most important predictor variables (Pueyo and Begueria, 2007). This information is not obtainable through a standard Markov model.

Finally, Lippe *et al.* (1985) tested a Markov model on an *Empetrum nigrum* heathland in the Netherlands, with the objective of determining whether the Markovian assumption held for that type of landscape. It was reported that the MC model did not support their dataset, primarily because of disturbances caused by insects and climate.

The disturbances caused changes in the transition matrix which is not accounted for in a simple Markov model (Lippe *et al.*, 1985). An inhomogeneous model, as was tested by Benabdellah *et al.* (2003) is one way of accounting for this. Lippe *et al.* (1985) also acknowledged that temporal trends in the transition matrices are not accounted for. They document a methodology in which the Markov model can be adjusted to account for these problems but would also cause the model to lose its simplicity.

2.4.3 Cellular automata Markov chain analysis

CA-Markov models combine the stochasticity of the Markov chain with the spatial dependence of the CA model. Balzter *et al.*, (1998) define these models as having spatial and temporal dependence. The spatial component is introduced through the neighbourhood of the CA, while the temporal aspect is incorporated through the Markov analysis. Several studies have used CA-Markov models to predict future land cover conditions.

Silvertown *et al.*, (1992) used a 40 by 40 lattice of square cells to model competition between five different species of grass. The state of a cell was dependent upon a Von Neumann neighbourhood at time $t-1$, and a set of rules that defined the extent of invasion for each species. This model used the transition matrix from the Markov model, and incorporated the spatial dimension by using real data. They found that the model with a random initial starting scenario was a good representation of the spatial arrangements used in standard competition experiments.

Balzter *et al.* (1998) modelled population dynamics of three plant species on a lawn. They found that the CA-Markov approach successfully modelled one species, but

the others were subject to selective grazing by an expanding rabbit population. The assumption that transition matrices were stationary over time is no longer valid, and the model did not simulate those species accurately.

2.5 Literature Review Summary

The review of the literature suggests that the objectives of this study can be achieved with methods applied by other researchers. Different combinations of topographic variables have proven to be effective predictors of where vegetation is likely to grow in the landscape. Given high classification accuracies, post-classification image comparison is one of the better digital image change detection methods. A CA-Markov hybrid model incorporates temporal and spatial dependence and presents an opportunity to incorporate Bayesian probabilities as a method of defining suitable areas of growth.

3. Data Sources

3.1 Field Data

Field data were collected between August 5th and August 14th, 2008. The vegetation survey is used to classify the satellite data, which provides the input for change detection analysis. The stratified random sample (Figure 3.1) was selected based on variations in aspect, elevation, and spectral signature of the 2001 Landsat image. This ensured that samples were taken at different topographic positions and for varying vegetation types. During the field season, 90 sites (Figure 3.1) were visited at which the IPY CiCAT protocol for mapping arctic vegetation was implemented (Chen, *et al.*, 2007). At each site, 1m² quadrats were placed 10m from a centre coordinate in each of the four cardinal directions (Figure 3.2). One of the intermediate directions, (NE, NW, SE, or SW) was selected randomly to be the location of the fifth quadrat at each site. The CiCAT protocol ensured appropriate coverage of an area that corresponded with satellite imagery at 30m resolution. At each quadrat, the following data were recorded:

1. Plant species present
2. Ground cover of each species (%)
3. Average height for each species (measured in cm from the base to the tallest stem on random samples in each plot).
4. Approximate soil depth (cm)
5. Aspect
6. Elevation (m), latitude and longitude recorded from GPS
7. A colour, vertical photograph of each quadrat

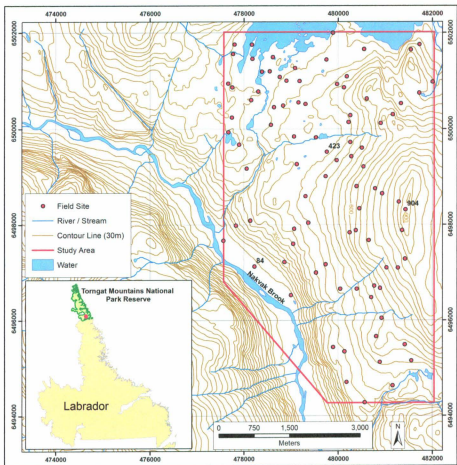


Figure 3.1. Field locations visited between August 5th and August 14th, 2008.

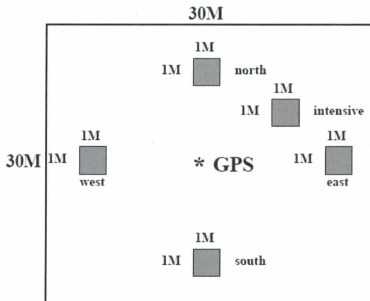


Figure 3.2 Plot scheme for arctic tundra regions. Source: Chen, *et al.*, 2007.

Satellite image classification was performed using identification of plant species and colour photographs as the primary information source. Identifying each plant species individually, enabled the vegetation to be aggregated into different classes used in this study. A DEM (1:50,000) provided the elevation and aspect values used in the analysis and the ground truth data were critical to the accuracy assessment of the classification and the certainty attained in the final model. Vegetation height and approximate soil depth were not specifically used in the analysis.

Presence of vegetation was initially recorded at the species level such that land cover classes could be aggregated and defined. Because of the accessibility and temporal scale of Landsat imagery, a spatial resolution of 30m was selected to classify land cover

(Chen, *et al.*, 2007). This resolution, combined with vegetation zone descriptions from Meades (1990) and recommendations given by Dr. Luise Hermanutz (2009)¹, was used to define three different land cover classes. Three broad classes of heath/grasses and sedges (HG), deciduous shrub (DSH) and rock/bare ground (RCK) were used in the analysis. Additional classes were initially developed such as separate classes for heath and grasses, but their spectral signatures showed little separability. This was partly due to the existence of multiple vegetation types within a 900m² area. The 30m resolution of the Landsat imagery was too coarse to classify those vegetation types separately.

The three remaining classes represent three broad groups of land cover that are well defined and distinguishable from one another. Table 3.1 provides a description and defining characteristics along with the common vegetation types found within each class. The HG class is the most difficult to define because of its coexistence with the RCK class. The DSH class is much easier to distinguish because there is a clear difference from HG and RCK classes. These classes allowed for adequate classification accuracy while maintaining the ability to observe whether temporal changes in vegetation occurred.

¹ Personal communication, Dr. Luise Hermanutz, Department of Biology, Memorial University of Newfoundland (2009).

Table 3.1 Land cover classifications used in this project (Typical plots for each land cover are shown on the right).

Class	Dominant Vegetation	Description / Defining Characteristics	Photograph (1m ² quadrat)
HG	<ul style="list-style-type: none"> -Grasses / sedges -Dwarf Labrador Tea (<i>Ledum palustre</i>) -Bilberry (<i>Vaccinium uliginosum</i>) -Diapensia (<i>Diapensia lapponica</i>) -Dwarf Birch (<i>Betula glandulosa</i>) -Dwarf Willow Species (<i>Salix spp.</i>) 	<ul style="list-style-type: none"> -Low growing vegetation -Presence of alpine species such as <i>Diapensia lapponica</i>. -Often a mixture of rock and HG found together. 	
DSH	<ul style="list-style-type: none"> -Balsam Poplar (<i>Populus balsamifera</i>) -Mountain Alder (<i>Alnus crispa</i>) -Willow Species (<i>Salix spp.</i>) 	<ul style="list-style-type: none"> -Species can grow up to 3m in height. -Found at lower elevations. -Fewer dominant species present 	

Table 3.1 Continued			
RCK	-None	<p>-Frost shattered rock often having moss and lichen growth</p> <p>-Often mixed with species from the HG class</p>	

3.2 Satellite Imagery

Four satellite images were obtained for the study site. A Landsat-5 Thematic Mapper (TM) image taken on August 9, 1985 was the earliest image available. Additional imagery included a Landsat-5 TM from August 5, 1992 and a Landsat-7 Enhanced TM (ETM+) from August 22, 2001. The final image of the time series was recorded on July 21, 2008 using the Satellite Pour l'Observation de la Terre (SPOT). This time frame corresponds closely to the vegetation survey field season. All of the Landsat images were recorded at 30m resolution while the SPOT image was recorded at 10 m resolution. The

SPOT image was re-sampled to 30m resolution in order to comply with the IPY CiCAT protocol (Chen, *et al.*, 2007). Each image was recorded during summer months when vegetation would have been at, or near its maximum growth for the season. This ensured that the vegetation types are in a similar state in each image and seasonal variations are minimized in the analysis.

Pre-processing of the satellite imagery involves geometric, atmospheric, and radiometric corrections. Each image is geometrically corrected with half pixel accuracy, to the 1:50 000 National Topographic System (NTS) map sheets. Atmospheric corrections were performed using the dark object subtraction method (Chavez Jr., 1996), which is based on the assumption that pixels in complete shadow or areas of clear, deep water should have no reflectance. Thus, any radiance received at the satellite sensor, over areas of dark shadow or deep water, is caused by atmospheric scattering. Subtracting this radiance value from the entire image, accounts for atmospheric scattering in the satellite image. Finally, the multi-date image normalization technique was applied for radiometric calibration. This method uses regression analysis to co-calibrate the spectral characteristics of satellite images obtained on different dates (Hall *et al.*, 1991). The applied correction allows for the imagery to be compared to one another because the detected changes will not include radiometric inconsistencies.

3.3 Image Classification

Each image in the time series was classified using a maximum likelihood algorithm. The dataset was split into two sets of 45 points so the field data could be incorporated into both the training and reference sites. Polygons were digitized around each point in the

training dataset to include nearby pixels, which corresponded to the land cover represented by that point. This increased the number of pixels from which training data could be extracted. In the reference dataset, only the pixel corresponding to each sampling site was digitized. The classification of each pixel was verified with the help of a colour aerial photograph, recorded in 2005 at a 1m spatial resolution, along with the photographs taken in the field and the record of species present for each plot. In order to increase the size of these small datasets, an additional 45 points were randomly generated for both the training and reference data. Each of those points was classified using only the aerial photograph as a reference. Points where the land cover was not definitive were removed from the dataset. The additional points resulted in 63 polygons being used for the training sites, and 70 for the reference points. Signature data generated from the training sites were used to classify each satellite image, while the reference sites were used to perform an accuracy assessment for each classification.

3.3.1 1985 Classification

This section discusses the 1985 image classification because of an area of misclassified pixels that were identified in the output. As a result, three different versions of the 1985 classification were compared. The accuracy assessment for the 1985 classifications is presented using producer's accuracy (omission error) and user's accuracy (commission error). Producer's accuracy gives the probability of a reference pixel being correctly classified, whereas user's accuracy is the probability that a classified pixel actually represents that particular class on the ground (Congalton and Mead, 1983). The accuracy assessment for the classifications of the remaining satellite imagery is also provided.

The initial classification of the 1985 image contained some commission errors for the DSH class that required further processing of the training data (Table 3.2). RCK had both high commission and omission errors. Overall kappa for the classification was 64.4%, a reasonable value considering the ground truth data were from 2008 and the image was recorded in 1985. There were also no aerial photos available from 1985 to help identify vegetation classes. The kappa value measures the relationship of the agreement beyond chance, with the expected disagreement. It is a robust accuracy measurement because it incorporates all of the cells in a matrix and not just the diagonal (Rosenfield and Fitzpatrick-Lins, 1986). The area highlighted in blue in Figure 3.3 is considered to be a problem because it is separate from the region where DSH is expected to be found and was not present in any other classification. Based on field observations, there was no evidence that DSH ever grew in that location. One method of correcting this problem was to perform image purification with image processing software. This reduces the effect that the problem area would have on subsequent analysis.

Table 3.2 Vegetation accuracy for original 1985 classification

Classification	Reference					
		HG	DSH	RCK	User's Accuracy (%)	Commission Error (%)
	HG	42	0	6	87.5	12.5
	DSH	2	6	0	75.0	25.0
RCK	4	1	12	70.6	29.4	
Producer's Accuracy (%)	87.5	85.7	66.7			
Omission Error (%)	12.5	14.3	33.3			

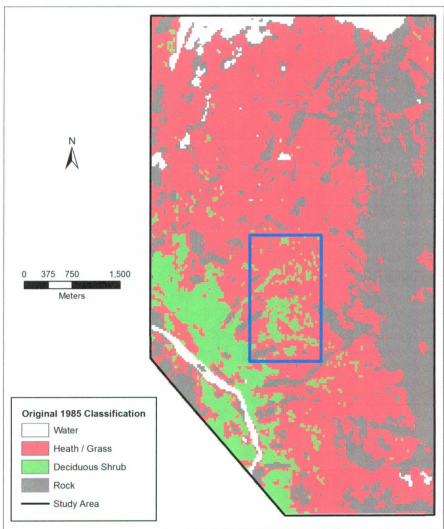


Figure 3.3 Original classification for 1985. Problem area is outlined in blue.

The nonparametric method of image purification removes outliers from the training sites used to create the classification. Cluster analysis was first used to define the entire image as one of the three previously defined clusters. Original training sites were used to define the locations under consideration in the cluster output. The areal proportion of each training class was calculated, and a decision to retain or discard a pixel was determined using a defined areal threshold. If any class has a proportion that is less than or equal to the areal threshold, the pixels are removed from the purified training sites. A combination of the purified training sites and the original training sites was used for the classification. The original training sites for HG and the purified sites for DSH and RCK were used in the final classification. Those three spectral signatures exhibited the greatest amount of separation and were more likely to yield a better classification. The purified classified image is presented in Figure 3.4. The problem area outlined is still a significant issue in the purified image, although the area is smaller compared to the original output image. The cross-classification matrix shown in Table 3.3 indicates that there was a negligible change in per-class accuracy and the overall kappa was 64.8%. This shows there was little to no change in classifications, which was partially due to the limited number of reference points. The purification process did not correct the area of DSH near the centre of the image.

Further analysis of the problem area used an iterative, self-organizing, cluster analysis was performed on the image to identify different clusters of signatures. Eleven clusters were generated and the cluster that made up the majority of the problem region was removed from the classified image. The missing data from that classification were then interpolated using indicator kriging.

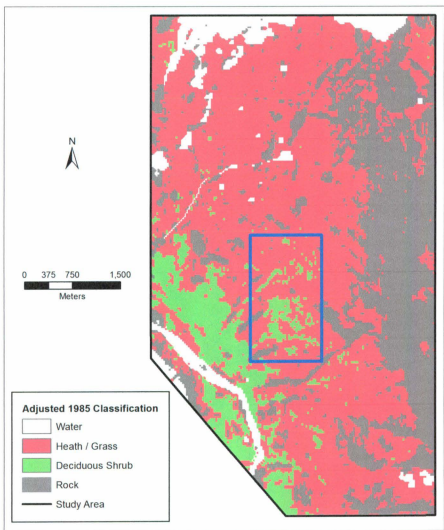


Figure 3.4 Purified classification for 1985.

Table 3.3 Vegetation accuracy for purified 1985 classification

Classification	Reference					
		HG	DSH	RCK	User's Accuracy (%)	Commission Error (%)
	HG	41	0	6	87.2	12.8
	DSH	2	6	0	75.0	25.0
RCK	4	0	11	73.3	26.7	
Producer's Accuracy (%)	87.2	100	64.7			
Omission Error (%)	12.8	0	35.3			

3.3.2 Indicator Kriging

Indicator kriging was initially developed for modeling mineral deposits, but has since been adapted for interpolating missing data in satellite imagery (Rossi *et al.*, 1994; Van Der Meer, 1996). Indicator kriging uses a weighted linear average of available data to estimate unknown data. The method offers some advantages over traditional interpolation methods, whereby it utilizes both distance and geometry for weighting available data and minimizing the variance of the expected error (Rossi *et al.*, 1994). Indicator kriging was utilized to estimate the data at locations that were removed from the purified 1985 classified image.

Indicator kriging is useful for this analysis because it uses binary data as input and the output is given as a probability of exceeding a user defined cut-off value (Babish, 2006). The area of interest in this case is located in an HG dominated area, so the image was reclassified to give all areas of HG, a value of 1 and all areas of DSH and RCK, a

value of 0. The specified cut-off value was then set to 0 such that indicator kriging would output the probability of exceeding 0, or the probability of being HG.

A random sample of 10 000 points was created for the classified image from 1985 and assigned a corresponding value 1 for HG areas and 0 for non HG areas. The output surface indicating the probability of finding HG in the area of interest is presented in Figure 3.5.

Most of the area removed from the central part of the image, has greater than 50% probability of being HG (Figure 3.5). There are few pixels that are less than 50%. Most of the lower probabilities are located near the southwest corner of the study area where the DSH land cover is found. Using a cut off value of 50%, these missing pixels can be classified into HG, or not HG, and replaced in the 1985 classification. The pixels classified as not HG, were returned to their original classification from 1985. The resulting classified image is shown in Figure 3.6. The deciduous shrub patch located near the centre part of the image was reduced in size, thus the influence it would have on the final model was minimized. Based on field observations, this adjusted classification was a better representation of the landscape. There was no presence of woody stems or dead matter at the study site that suggested deciduous shrubs grew there recently. The cross classification matrix (Table 3.4) shows little improvement in classification accuracy, which can be attributed to low numbers of reference points. Overall kappa is the highest for this classification at 65.7% compared to 64.4% for the original and 64.8% for the purified classification. This suggests indicator kriging slightly improved the classification.

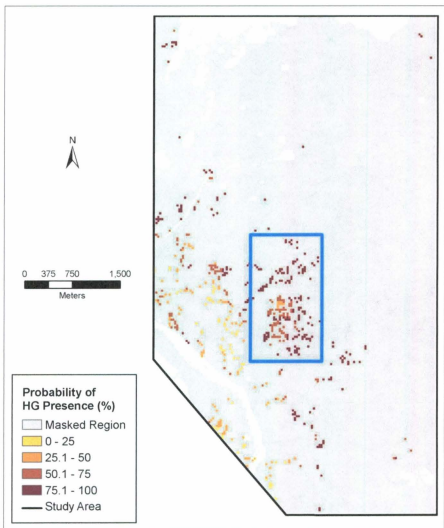


Figure 3.5. Probability of finding HG in the problem region of the 1985 classification

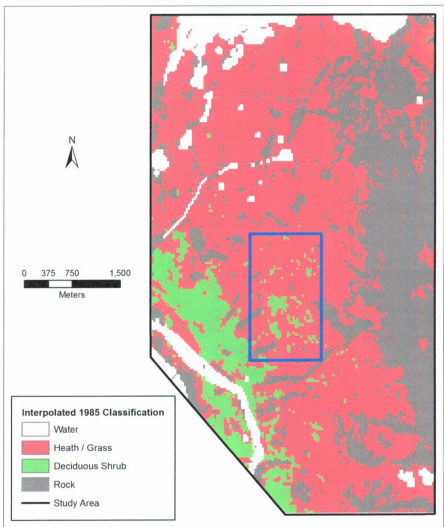


Figure 3.6. Maximum likelihood classification of 1985 Landsat MSS image. Indicator kriging was used to interpolate area that was removed from the signature analysis.

Table 3.4 Vegetation accuracy for the interpolated 1985 classification

Classification	Reference					
		HG	DSH	RCK	User's Accuracy (%)	Commission Error (%)
	HG	40	0	5	88.9	11.1
	DSH	2	6	0	75.0	25.0
RCK	5	0	12	70.5	29.5	
Producer's Accuracy (%)	85.1	100	70.5			
Omission Error (%)	14.9	0	29.5			

Error assessment of the interpolated model can be analyzed using the histogram, summary statistics of the errors, and by mapping the distribution of the errors (Rossi *et al.*, 1994). A perfect model would result in the mean, median, variance, and quantiles all being zero. These statistics were used to evaluate how well the model performed.

Table 3.5 lists the summary statistics for the model. Overall, these statistics suggest that the model was a good representation. The mean, median and variance all have very low values and the quartiles suggest that most of the error was between -0.142 and 0.114. This indicates that the errors are clustered in a low range of values. Of the 10 000 points used for the interpolation, 1291 had an error of 0 which accounted for 12.9% of the total sample. The small positive skewness value indicates that the model tends to have a small bias toward overestimated error. This was also evident in the histogram (Figure 3.7), which shows the overestimation as negative values and underestimation as positive values. The negative values represent points that were not HG but were estimated as being HG to some degree. The positive values represent points that

were HG but were estimated as having some probability of not being HG. The histogram shows that the highest frequencies of overestimation and underestimation occur among very low errors. This is an indication that the model provided a good representation of the data.

Table 3.5 Summary statistics of errors for the interpolated surface.

Summary Statistic	Value
Mean	0.000
Median	-0.010
Variance	0.100
Quartile 1	-0.142
Quartile 3	0.114
Skewness	0.340
Kurtosis	1.027

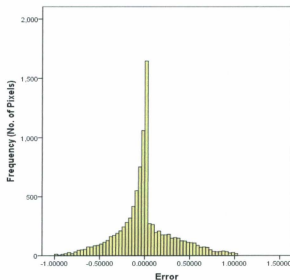


Figure 3.7 Histogram showing frequency of errors from kriged model.

The error values are also mapped for the interpolated area (Figure 3.8). Underestimated values are a little higher in the centre portion of the image but there were also some overestimated values in the same region. The over and underestimated errors were distributed randomly throughout the area of interest, as shown in Figure 3.8.

Overall, indicator kriging appropriately estimated the land cover for the area considered to be inaccurate in the 1985 classification. The patch of deciduous shrub outlined in Figures 3.3 – 3.6 was reduced in size and better represented the conditions observed in the field. The revised classification (Figure 3.6) provided a baseline classification for modelling vegetation change in the study area.

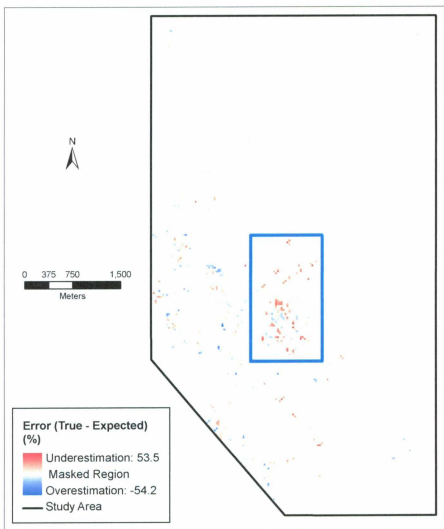


Figure 3.8 Overestimated and underestimated errors produced by the geostatistical model.

3.3.3 1992, 2001, and 2008 classifications

The classifications for the remaining three images did not require any special consideration. This is partly because the imagery is more recent, and allowed for more accurate representations of the ground cover. Each image was classified using the maximum likelihood algorithm. Cross-classification matrices for each of the classifications from 1992, 2001 and 2008 are presented in Tables 3.6 – 3.8. There are still some commission errors in the classifications, but overall kappa values improved with 80.2%, 88.2% and 86.2% respectively. Per-class Kappa Index of Agreement (KIA) values was also very high. Table 3.9 compares the per-class KIA values for the each of the classifications. It is evident that the per-class KIA values are much higher for the more recent imagery, than for any of the 1985 imagery. The per-class accuracies were also used to account for error in the Bayesian analysis by multiplying the accuracy value by the Bayesian probability. These KIA values are used to account for certainty in the Bayesian analysis and the final CA-Markov model.

Table 3.6 Vegetation accuracy for the 1992 classification

		Reference				
		HG	DSH	RCK	User's Accuracy (%)	Commission Error (%)
Classification	HG	42	0	2	95.4	4.6
	DSH	2	6	0	75.0	25.0
	RCK	3	0	15	83.3	17.7
Producer's Accuracy (%)		89.4	100	88.2		
Omission Error (%)		10.6	0	11.8		

Table 3.7 Vegetation accuracy for the 2001 classification

		Reference					
Classification		HG	DSH	RCK	User's Accuracy (%)	Commission Error (%)	
	HG	45	0	2	95.7	4.3	
	DSH	0	6	0	100	0	
	RCK	2	0	15	88.2	11.8	
Producer's Accuracy (%)		95.7	100	88.2			
Omission Error (%)		4.3	0	11.8			

Table 3.8 Vegetation accuracy for the 2008 classification

		Reference					
Classification		HG	DSH	RCK	User's Accuracy (%)	Commission Error (%)	
	HG	42	0	0	100	0	
	DSH	2	6	0	75.0	25.0	
	RCK	3	0	17	85.0	15.0	
Producer's Accuracy (%)		89.4	100	100			
Omission Error (%)		10.6	0	0			

Table 3.9 Kappa Index of Agreement (KIA) values for all classifications

	HG	DSH	RCK
1985 Original	0.635	0.840	0.565
1985 Purified	0.611	1.000	0.551
1985 Interpolated	0.583	1.000	0.611
1992 Classification	0.714	1.000	0.842
2001 Classification	0.870	1.000	0.845
2008 Classification	0.734	1.000	1.000

The classifications are presented in Figures 3.9 - 3.11. The most noticeable difference between these and the 1985 classification is the large area of DSH outlined in Figures 3.3 (Page 34). The patch is missing from all three more recent classifications. DSH is located at lower elevations in the southwest region of each image, with very little presence elsewhere. This is evidence that the patch of DSH in the centre of the 1985 images is an anomaly. The middle portion of the classification is comprised primarily of the HG class. The area is representative of elevation ranging from approximately 300m to 700m. RCK is the dominant class above this elevation and located in the eastern part of the image. Visually, all images are somewhat similar, indicating there has not been any dramatic change in vegetation. The 2008 image tends to have more of a speckled appearance, particularly with the mixture of HG and RCK classes. This is an artefact related to the original 10m resolution of the SPOT image.

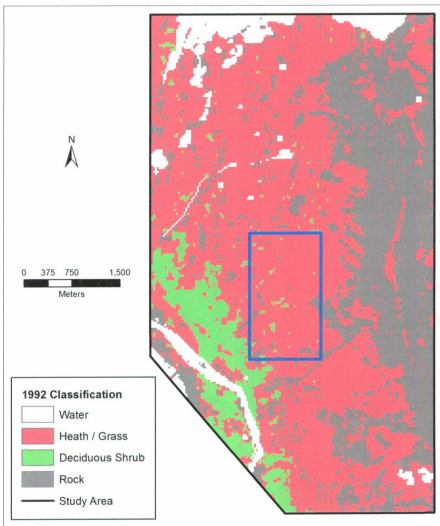


Figure 3.9 Maximum likelihood classification for 1992 Landsat 5 TM image.

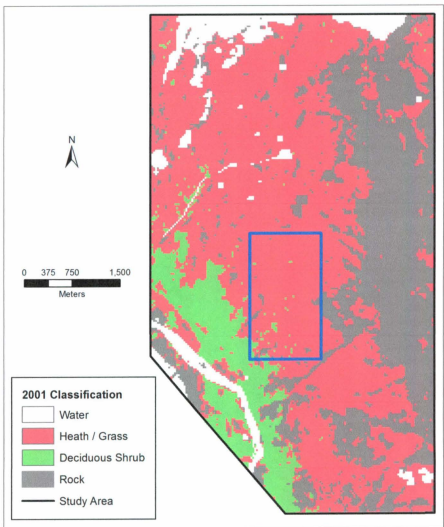


Figure 3.10 Maximum likelihood classification for 2001 Landsat 7 TM image

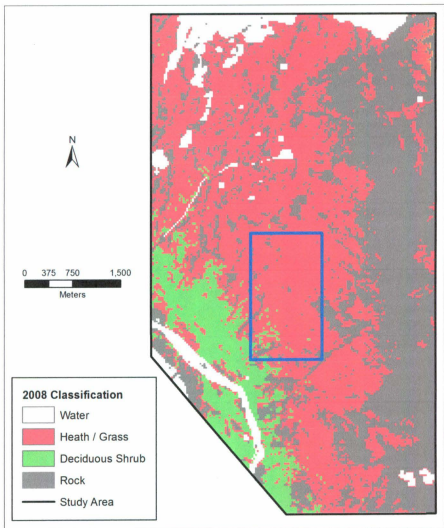


Figure 3.11 Maximum likelihood classification for 2008 SPOT image

3.4 Topographic Variables

Topographic variables are used in predictive vegetation mapping as a way to describe the landscape and also as independent variables in statistical models. The majority of predictive vegetation models use elevation, aspect, and slope as variables (Franklin, 1995). These variables are utilized in this project along with two additional variables. The first is a relative moisture index (RMI) that measures the moisture potential of the land, based on slope and flow accumulation (Moore *et al.*, 1993). The second variable is the topographic shape index (TSI) which represents the position along a slope. All of the topographic variables were created using map algebra in ArcMap 9.3.

3.4.1 Elevation

Elevation is directly related to the growth of vegetation because of its association with temperature. The relationship between elevation and vegetation growth in tundra environments has been well established (Cannone *et al.*, 2007; Korner and Paulsen, 2004). Elevation was derived directly from a DEM, on which a 9 pixel by 9 pixel filter was applied to remove artefacts from the model. This produced a smooth surface from which other indices could be derived. Elevation ranged from approximately 75m in the valley near Nakvak Brook to a maximum of 915m.

The vegetation at all elevations is typical of the tundra elevational zone which consists of dwarf shrubs, grasses, mosses and lichens. Elevation classes are based on the distinct areas where each land cover class is located. Each elevation class is defined as the mean elevation plus one standard deviation for each vegetation class. The classes of elevation are displayed in Table 3.10. This method of classification is possible because of

the distinct locations of each vegetation class. Based on field observations, it was clear that DSH was dominant below 250m but not particularly abundant above that elevation. Mid elevations are dominated by HG and higher elevations are comprised mostly of rock. This method of classifying elevation is based on divisions observed in the landscape and is a general guideline describing the elevation divisions of the tundra landscape.

Table 3.10 Classification scheme for elevation.

Vegetation Class	Mean Elevation (m)	Standard Deviation (m)	Total (m) (Mean + SD)	Elevation Range (m)	Elevation Class
DSH	160	87	247	0 – 247	1
HG	433	123	556	247 - 556	2
RCK	N.A	N.A	N.A	556 - 915	3

3.4.2 Aspect

Aspect was calculated and classified using the original raster layer. Nine classes total were used for aspect. They corresponded to each of the four cardinal directions and the intermediate directions, along with a class for flat areas. The classification scheme shown in Table 3.11, displays the 45° intervals used to define the classes.

Table 3.11 Classification scheme for aspect based on equal interval divisions.

Aspect Interval (Degrees)	Direction	Aspect Class
337.5 – 0 – 22.5	N	1
22.5 – 67.5	NE	2
67.5 – 112.5	E	3
112.5 – 157.5	SE	4
157.5 – 202.5	S	5
202.5 – 247.5	SW	6
247.5 – 292.5	W	7
292.5 – 337.5	NW	8
Flat		-1

3.4.3 Slope

Slope is directly related to other variables such as exposure, soil moisture, and topography of the land. For the purpose of this analysis, slope was expressed as 'percent rise'. This is the rise in elevation divided by the horizontal distance, multiplied by 100. Percent rise is equal to 100% when the horizontal displacement is equal to the rise in elevation and can approach infinity when the slope approaches vertical.

Slope was reclassified into seven separate classes adapted from Dobos *et al.* (2005). The slope classification gradually increases from more gentle slopes to more extreme, steep slopes (Table 3.12).

Table 3.12 Classification scheme for slope adapted from (Dobos *et al.*, 2005)

Description	Slope (%)	Slope Class
Flat	0 – 2	1
Gently Undulating	2 -5	2
Undulating	5 - 8	3
Rolling	8 - 15	4
Moderately Steep	15 - 30	5
Steep	30 - 60	6
Very Steep	60 +	7

3.4.4 Relative Moisture Index

The Relative Moisture Index (RMI) provides a measure for moisture levels at a site when actual field data are not available. RMI calculates the relative amount of water flowing into a location, represented by one pixel, in relation to the amount flowing out to the locations represented by surrounding pixels. It is adapted from Moore *et al.* (1993) and is represented by map algebra Equation 3.1.

$$RMI = \ln((\text{flow accumulation} + 1) / (\text{Slope} + 1))$$

Equation 3.1 Relative Moisture Index

Flow accumulation represents the accumulated weight of all cells that flow into down-slope cells and is calculated using a raster layer showing flow direction. Flow direction is determined from a DEM.

The relative moisture index was classified based on Young (2006), who used a simple division of wet and dry. The classification adapted here uses wet and dry as a

guideline, but has equal interval classes between the extreme ends of the scale to create a gradient of wetness (Table 3.13).

Table 3.13 Classification scheme for RMI adapted from Young, (2006)

RMI Interval	Description	RMI Class
-10 to -2	Very Dry / Well Drained	1
-2 to -1	Decreasing Wetness 	2
-1 to 0		3
0 to 1		4
1 to 2		5
2 to 10		Very Wet / Poorly Drained

3.4.5 Terrain Shape Index

The Terrain Shape Index (TSI) is a measure of the convexity or concavity of the landscape. This index was adapted from McNab (1989), by taking the mean relative difference in elevation between a centre cell and its eight surrounding neighbors. It is given by Equation 3.2.

$$TSI = DEM - \text{Focal Mean} \quad \text{Equation 3.2 Terrain Shape Index}$$

Where a given DEM value is the centre cell and the focal mean is the average of the eight surrounding neighbors. The TSI can have values from negative to positive infinity. For this study area, the range was from -372 to 287.

The classification given in Table 13.14 is modified slightly from Zimmermann (2001) to account for the specific landscape of the study area. The index describes varying positions on a slope. Values increase with movement up-slope, so that the highest

negative values represent valley bottoms and highest positive values represent peaks or ridges. Values near zero are mid-slope positions.

Table 3.14 Classification scheme for TSI adapted from (Zimmermann, 2001).

TSI Interval	Description	TSI Class
-1000 to -200	Valley Bottom	1
-200 to -75	Toe Slope	2
-75 to 0	Mid Slope	3
0 to 150	Upper Slope	4
150 to 1000	Ridge	5

3.5 Landscape Description

This section relates the three land cover classes with the topographic variables to gain an understanding of the distribution of vegetation in the landscape. Histograms for each topographic variable are categorized by land cover class to show the differences between classes.

Elevation was divided into 20m intervals to show variability in the histogram. The small elevation intervals show in detail where the vegetation classes occur. The result (Figure 3.12) shows that each of the three land cover classes is dominant at different elevations. The DSH class occurs primarily below 240m with relatively low levels of occurrence above that elevation. DSH also has the most limited elevation range of the three classes as is shown by the statistics of Table 3.15. HG is dominant between approximately 340m and 500m, but is found throughout the entire landscape below 850m. RCK has the largest range of the classes because it is found at every elevation. Although

frequencies of RCK in the 440-600m and 700-900m ranges are similar, it is at the higher elevations where RCK is the dominant land cover.

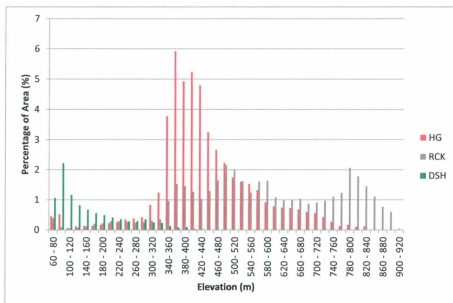


Figure 3.12 Histogram of elevation per land class.

Table 3.15 Elevation statistics for each land cover class.

	Mean (m)	Standard Deviation (m)	Minimum (m)	Maximum (m)	Range (m)
DSH	160.8	87.1	59.1	478.3	419.2
HG	433.9	123.1	59.2	849.7	790.5
RCK	576.8	184.4	60.8	902.6	841.8

The histogram for aspect was divided into eight cardinal direction classes (Table 3.11). Figure 3.13 illustrates that westerly facing slopes dominate this landscape. Highest occurrence levels for all three land covers are located in a western direction. The histogram does show that DSH is nearly absent from NW facing slopes even though HG and RCK maintain the higher pixel counts in this category. The low values for DSH along generally north facing slopes indicate that lower amounts of sunlight associated with these areas may inhibit DSH from growing. HG appears to grow in every aspect and RCK occurs in every part of the landscape.

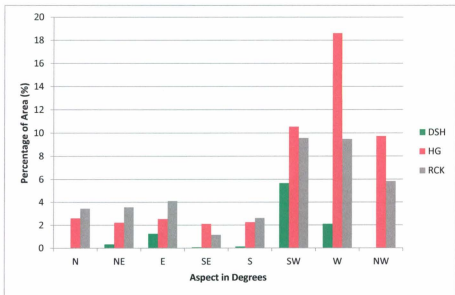


Figure 3.13 Histogram showing distribution of aspect per land class.

The histogram showing the relationship between slope and the land cover classes (Figure 3.14) illustrates that the majority of slopes are between 8% and 30%. This corresponds to rolling or moderately steep areas presented in Table 3.12. The highest occurrence of DSH occurs on slopes in the 30-60% range which suggests that a steep slope does not restrict the growth of DSH. Its occurrence along the valley wall, which make up most of the 30-90% slopes, has not prevented DSH growth along these slopes. So, based on this distribution, it is plausible that DSH can overcome steep inclines and move into upslope regions provided soil and aspect provide a suitable habitat.

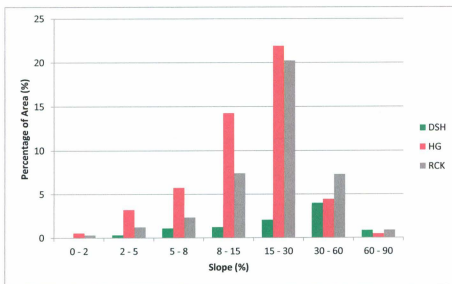


Figure 3.14 Histogram showing the distribution of slope per land class.

The distribution for the relative moisture index (Figure 3.15) shows that DSH and HG will grow equally well in all moisture levels. Higher occurrences of HG are found in intermediate moisture areas and there is a slight skewness showing that RCK is found more in dry, well-drained areas.

Figure 3.16 displays the distribution of the topographic shape index (TSI). This index shows the positioning of a land cover on a slope and it is clear that DSH is found primarily on the middle to lower portion of the hills. HG is more dominant in the mid and upper slopes while RCK dominates the ridges. This is similar to observations for elevation (Figure 3.12) because the TSI is a composite of terrain characteristics.

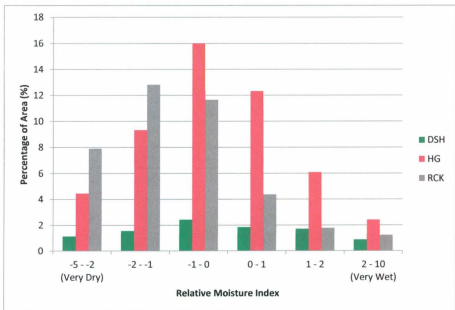


Figure 3.15 Histogram showing the distribution of RMI per land class.

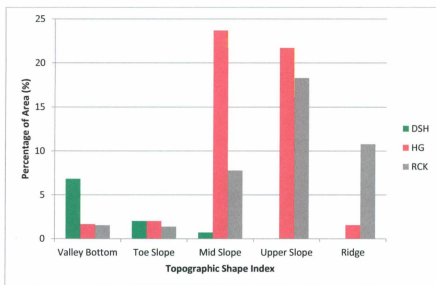


Figure 3.16 Histogram showing the distribution of TSI per land class.

3.6 Climate Data

It is difficult to obtain complete and accurate datasets of historical climate for northern regions of Canada. Sparsely located climate stations, irregular maintenance schedules, and adverse weather conditions all contribute to climate data being either incomplete, or absent for a particular region. A potential solution to this problem is using interpolated datasets to estimate temperature and precipitation values at the study site. Hutchinson *et al.* (2009) used a trivariate, thin-plate smoothing spline to model daily temperature and precipitation, for all of Canada. Model resolution was 300 arc seconds (9258m) of latitude and longitude and they report that errors for northern Canada were significantly larger than those in southern Canada. Root mean square errors for maximum temperatures ranged from 1.45°C to 2.37°C (Hutchinson *et al.*, 2009). For each sample point in Figure

3.1, mean maximum and mean minimum temperatures for 1970 to 2007 were supplied by Dr. Dan McKenney (2009)². The dataset represents the best climate data available for the study area because it provides complete coverage over the entire time period and has reasonable errors of estimate associated with it. More accurate data is desirable; however this is only possible if there were more climate stations in northern regions.

The data were supplied in point form for each of the field survey locations displayed in Figure 3.1. It was interpolated to raster format using an inverse distance weighted algorithm. The raster layers were subsequently used to examine trends and patterns in changing temperatures and to compare trends in vegetation change.

3.7 Summary of Data

Topographic and vegetation cover data are required for change detection analysis and predictive modelling. A vegetation survey enabled plants to be identified and quantified as percent cover. Each image was classified into DSH, HG, and RCK classes using a maximum likelihood algorithm. Anomalous areas in the 1985 classification were minimized using indicator kriging and a classification accuracy of 65.7% was attained. The classifications for 1992, 2001, and 2008, had accuracies of 80.2%, 88.2%, and 86.2% respectively. The lower accuracy for 1985 occurred because the 1985 classification was generated using 2008 field data. The difference in classification accuracy is an indication that vegetation change has occurred. Topographic variables describe the landscape and the conditions in which different vegetation will grow. Elevation, aspect, slope, topographic shape, and relative moisture were used to describe the vegetation distribution

² Personal Communication, Dr. Dan McKenney, Canadian Forest Service, Great Lakes Forestry Centre (2009).

and will be used to define suitable areas for growth. Interpolated climate data are the most complete dataset available for northern regions of Canada. They will be used to assess trends in temperatures compared to observed changes in vegetation.

4. PRELIMINARY RESULTS

4.1 Change Detection

Change detection analysis was applied to classified satellite data, as well as climate data for this project. The post-classification comparison provided information concerning net change, for each land cover class. The climate change detection procedure was effective in establishing the trends in temperatures for the study area and providing some insight into changes in the length of the growing season. These applications are discussed in full detail in the following sections.

4.1.1 Post-classification image comparison

Predicting future changes of vegetation patterns can only be done if historical data provides evidence that changes have occurred in the past. This information is required for any spatial models dealing with changes in natural land cover. Post-classification image comparison is used to verify whether vegetation distribution in the Torngat Mountains has changed since 1985. Additionally, change detection was applied to quantify the amount of change expected in the future. This information is used to verify whether spatial models will provide reasonable estimates of future predictions.

The focus of this project was to detect land cover changes between 1985 and 2008. This was the longest time frame for which data was available to observe vegetation change. Intermediate years of 1992 and 2001 were also assessed in order to observe trends over the time series. Jia *et al.*, (2009) found vegetation greenness in the Arctic changed on a decadal time scale between 1982 and 2006 thus the time scale for this

research is appropriate. It should be noted that the interpolated version of the 1985 classification was used for this and all further analysis.

Initially, one should describe the current conditions of each vegetation class observed in the study area. Table 4.1 outlines the area in km² for each vegetation class in 2008 as well as the percent area for the entire study region. It is clear that the region is made up primarily of HG and RCK.

Table 4.1 Proportion of land cover class present in 2008.

Land Cover Class	Area (km ²)	Proportion (%)
HG	14.82	50.34
DSH	2.81	9.54
RCK	11.81	40.12
Total	29.44	100

Change in total area of each vegetation class is presented in Figure 4.1. The graph shows that the HG class is the most abundant vegetation type followed by RCK and DSH. The HG class had a gradual decrease in area over the extent of the time series. This resulted in RCK being exposed and therefore RCK experienced an increase. Figure 4.2 has a more suitable scale for DSH and shows that it has an increasing trend. There is not a continuous upward trend, although there is a clear increase in area when comparing the earlier classifications with the later classifications.

Figures 4.1 and 4.2 show that comparing the 1985 and 2008 classifications will yield the greatest difference in area for any vegetation class. The exception here is DSH

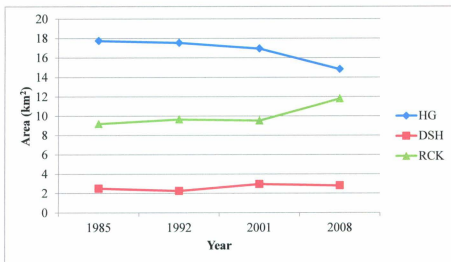


Figure 4.1 Total area of each land cover class for classification in the historical time series.

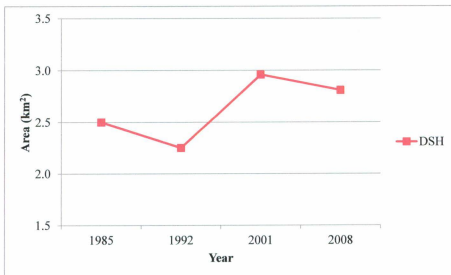


Figure 4.2 Total area for DSH class over the time series.

where 1992 and 2001 have the greatest difference. Consecutive images tend to have less difference between them which is indicative that changes are occurring on a decadal time scale. To interpret changes in the landscape, it is best to look over a timescale of at least ten years. At this time interval, it is more likely that significant change will be observed. For this reason, the majority of the remaining change analysis was performed using the 1985 and 2008 classifications. This provided twenty-three years over which change could be observed and provided the best opportunity for detection.

Further analysis of the changes in area, was examined through gains and losses of each land cover class between 1985 and 2008 (Figure 4.3). RCK had the largest increase in area, relative to the amount of area that was lost while HG had a larger decrease than increase. DSH experienced a net gain in area but the change was much smaller than those observed for RCK or HG. This was expected due to the relative proportions of each class. Figure 4.4 shows that the vast majority of change occurred between RCK and HG, with DSH accounting for the remaining net change. Since the total area of the DSH is only 2.81 km² in 2008, 0.30 km² represents a 10.7% increase in the total area. This is comparable to a 22.2% increase for RCK and 19.7% decrease in total area for HG.

The following paragraphs discuss the spatial pattern of vegetation change in the study area. The HG class experienced a loss in area over the twenty-three years. Figure 4.5 shows the distribution of the gains and losses in this class between 1985 and 2008. These results contradict those found by other studies (Canone *et al.*, 2007; IPCC, 2007). This is related to low joint classification accuracies of the HG (42.7%) and RCK (61.1%) classes in the 1985 classification.

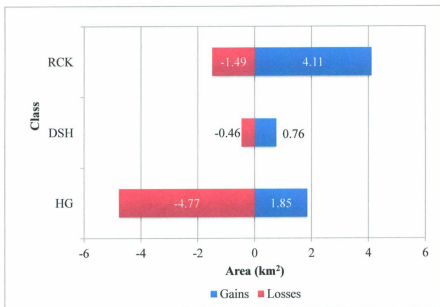


Figure 4.3 Total area gained and lost between 1985 and 2008 for each land cover class.

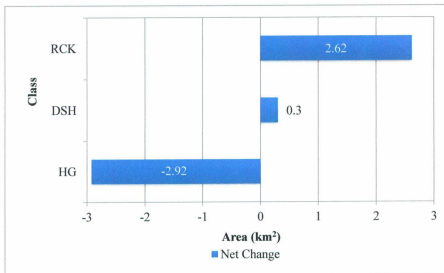


Figure 4.4 Net change for each land cover class between 1985 and 2008.

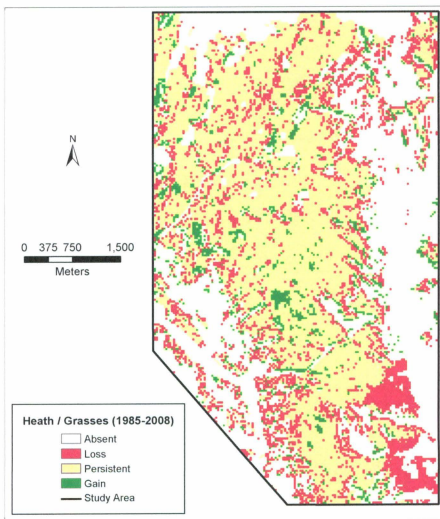


Figure 4.5 Areas of gains and losses of HG class between 1985 and 2008.

Inaccuracies in classification may be caused by mixing between the HG and RCK classes. Areas where these classes coexist can be classified differently due to reflective differences of the landscape and without field data from 1985, it is difficult to achieve better classification accuracy for 1985.

The pattern for gains and losses of DSH is confined to lower elevations in the southwest corner of the study area. Figure 4.6 shows that the majority of losses are located among the region toward the centre of the image where the classification issues were identified. This region had its extent minimized but still impacted the change analysis. Aside from the larger clusters of pixels that indicate a loss, there are very few areas where a loss in DSH was detected. Most of the change in DSH indicates that there was growth in the region. The pixels are primarily located along the edges of persistent shrubs where change is expected to occur. This change indicates that the shrubs expanded their extent and began moving upslope into higher elevations. The persistent DSH area from Figure 4.6 had a mean elevation of 141.1 m while the areas of gain had a mean elevation of 203.0 m. It is evident from those values that the areas of gain had been growing at higher average elevations. Visually, most new growth appears to occur on the northeast edge of the persistent DSH.

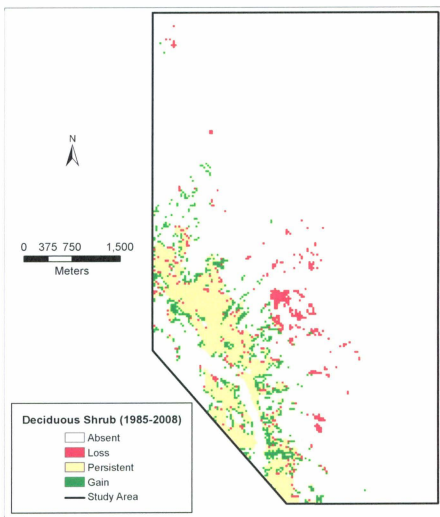


Figure 4.6 Areas of gains and losses in DSH between 1985 and 2008

4.1.2 Climate change assessment

The climate data provided by Dr. Dan McKenney (2009) were used to calculate mean monthly temperatures from 1985 to 2007. The time series, which nearly covered the temporal span of the satellite imagery, was used to assess the interannual and seasonal trends in temperature.

The median trend in average temperature was analyzed to determine if a warming trend could be observed in the data. It was calculated using a Theil-Sen median trend operator which determines the slope between every pairwise combination in the time series and then calculates the median (Eastman, *et al.*, 2009). This method of determining trends in a time series is recommended when a dataset is very small or noisy. In the case of this time series, the Theil-Sen median trend was utilized because the data represented a small sample size of twenty-two years. Figure 4.7 shows the trend over the extent of the study area. The region in the eastern part of the image, at higher elevation, warmed faster than the western area however, the difference in temperature is 0.24°C . This is less than the RMSE values of 1.45°C to 2.37°C , which was reported by Hutchinson *et al.* (2009) so there is no certainty in the difference between the temperatures at different elevations. The warming trend is also evident by looking at mean annual temperatures and applying a linear trend to the data (Figure 4.8). These values are similar to the temperature increases reported by the Arctic Climate Impact Assessment (ACIA). They showed an average temperature increase of 1.06°C per decade for North America between 1981 and 2001 (ACIA, 2005). Given those values, an increase of 2.8°C to 3.0°C is at the upper limit of expected warming for the twenty-two year time period.

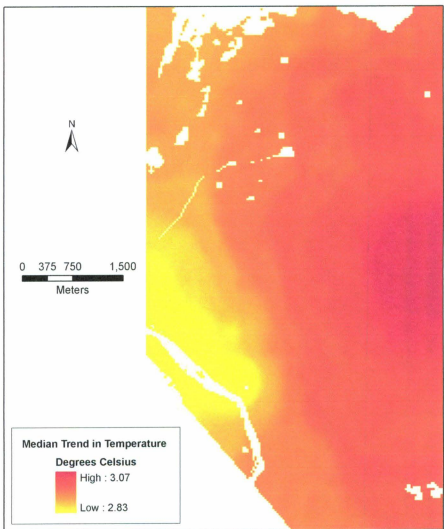


Figure 4.7 Theil-Sen median trend in temperature. Represented as total change in temperature over the twenty-two year time series.

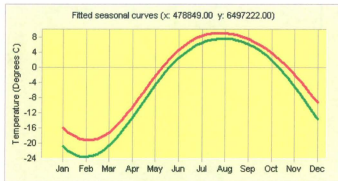


Figure 4.8 Fitted seasonal curves for 1985-1991 (green) and 2001-2007 (red). Differences between curves represent average changes in temperature between time periods.

Seasonal trends are analyzed by assessing the shape of the seasonal curve over the extent of the time series (Eastman, *et al.*, 2009). The result of this analysis focuses on a small area in the valley, where the lowest temperature increases were observed. This area corresponds to the location where DSH existed in 2008 and provides an indication whether climate change is also evident with corresponding vegetation movement upslope. The lack of temperature variation in this area makes it a reasonable representation of the entire study region. Harmonic regression was applied to the time series to extract the mean annual temperature image and the annual cycle.

Two curves were initially fitted to the time series. One curve corresponds to the first seven years of the time series while the other corresponds to the last seven years (Figure 4.8). This was an appropriate interval for the twenty-two year time span because it provides a good representation of the beginning and end of the time series. The differences in the curves depict an increase or decrease in temperature from one time period to the next. Figure 4.8 shows a clear separation of temperatures between time

periods. The 2001-2007 temperatures remain above the 1985-1991 temperatures indicating that every month is warmer on average for the later part of the time series. These curves also provide a better indication of seasonal temperatures. The greatest warming has occurred during winter months. Temperatures are as much as 4°C warmer during January and February whereas temperatures in July and August are about 1°C warmer on average. Temperatures are also exceeding 0 °C earlier in the season which is demonstrated through green-up and green-down measurements. The approximate time period corresponding to spring and fall were set to green-up and green-down respectively. It was determined that the green-up period occurred approximately 10.7 days earlier in the 2001-2007 time period than it did from 1985-1991. The green-down period occurred approximately 11.3 days later than it did in the earlier time period. The effect of temperatures surpassing 0°C is evident in the length of the growing season which was approximately three weeks longer between 2001 and 2007 than it was between 1985 and 1991. This indicates that there is greater potential for vegetation to occupy a larger spatial extent and to become more dominant in areas where it currently exists.

Mean annual temperatures were calculated for the time series and a Theil-Sen slope was applied as a trend line to visualize change in temperature. This is referred to as 'amplitude 0' and is shown in Figure 4.9. The trend in the data show an increase of approximately 3°C overall. Additionally, the data suggests that there is a trend in the annual difference between winter and summer temperatures. This is represented in Figure 4.10 as 'amplitude 1'. The graph has a decreasing trend, indicating that the difference between mean winter temperatures and mean summer temperatures is getting smaller.

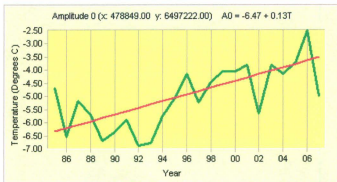


Figure 4.9 Amplitude 0 showing Theil-Sen slope indicating the trend in mean annual temperature.

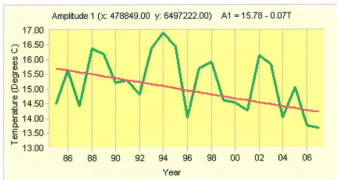


Figure 4.10 Amplitude 1 which shows the difference between winter and summer temperatures is decreasing on average.

This implies that winter season has experienced a greater amount of warming than the summer season and helps verify the observations of Figure 4.8, which shows winter temperatures warmed more than summer temperatures. The amplitude 0 and amplitude 1 graphs incorporate the entire time series rather than the first and last seven years.

To gain a general understanding of the relationship between vegetation change and observed climate change, mean average temperature and total area of each land cover class, were plotted in Figure 4.11. The increasing trend in temperature corresponds with the increase in area of RCK and inversely corresponds with HG. DSH has a small increasing trend indicating there is some association between DSH growth and increasing temperatures. Figure 4.11 indicates there could be some correlation between the dynamic vegetation patterns in the study site and changing temperatures, but these changes need to be monitored over decades to better understand the relationship.

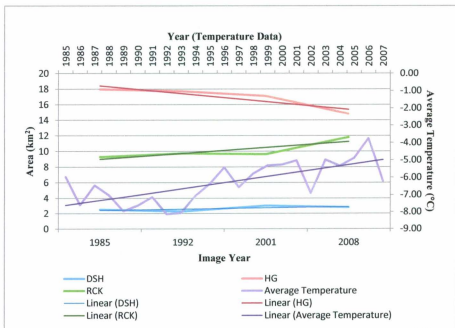


Figure 4.11 Trend in average mean temperature compared to change in area of vegetation class.

4.1.3 Summary of Change Detection Analysis

Post-classification image comparison was used to determine changes in vegetation cover over time. It was found that DSH experienced an increase in areal coverage whereas HG area decreased. Expanded areas of DSH occurred along persistent vegetation which suggests growth will occur near well established areas of DSH. Losses in HG occur along the boundary between HG and RCK however, those changes were associated with very low classification accuracies of the 1985 satellite image

Climate change was assessed using interpolated climate data and indicated that temperatures have warmed by as much as 3.0°C since 1985. On average, there are about twenty-two more days during the year that temperatures exceed 0°C, thus providing longer growing seasons for vegetation. The results suggest that DSH has potential to continue to expand in areas with these increased temperatures.

4.2 Bayesian Probabilities

Bayesian probabilities (B_{Prob}) were used in this study as a secondary method of change detection and to define suitable areas of growth in the cellular automata Markov chain (CA-Markov) model. Calculations were made for each land cover class for each satellite image. This enabled the B_{Prob} to be compared over time and allowed them to be input into the model on a per class basis. The method of calculating B_{Prob} and applying them to vegetation change detection is discussed in this section.

4.2.1 Calculating Bayesian Probabilities

Prior probabilities must be evaluated before calculating Bayesian probabilities. Prior probabilities represent the probability of finding a particular land cover class based on the existing coverage in the study region. These can be calculated by finding the proportion of each land cover class for each year using Equation 4.1

$$P_{Prior} = \frac{A_{LCi}}{A_{Tot}} \quad \text{Equation 4.1 Prior probability}$$

Where P_{Prior} is the prior probability, A_{LCi} is the area of a particular land cover class, and A_{Tot} is the total area of the study area. The prior probabilities for each land cover class for each year are given in Table 4.2, and are a general representation of the entire landscape for each year. B_{Prob} have the advantage of incorporating additional information to improve the prediction of land cover classes. For this research, the additional information comes in the form of the elevation, aspect, slope, relative moisture index and topographic shape index, variables presented in section 3.4. The variables describe where particular land cover classes exist, and can be used to help predict the most likely areas where these land cover classes will exist in the future. The calculation of B_{Prob} requires the assumption of conditional independence which means that each topographic variable included in the calculation are considered independently from one another (Bonham-Carter, 1994). B_{Prob} were calculated for each land cover class using a simplification of Bayes Rule shown in Equation 4.2.

$$P(LC_{ij}|T_E \cap T_S \cap T_A \cap T_{TS} \cap T_M) = \frac{P(LC_{ij} \cap T_E \cap T_S \cap T_A \cap T_{TS} \cap T_M)}{P(T_E \cap T_S \cap T_A \cap T_{TS} \cap T_M)}$$

Equation 4.2 Bayesian probability (Bonham-Carter, 1994).

Where: LC_{ij} = a particular land cover (i) for a particular year (j)

T_E = Elevation

T_S = Slope

T_A = Aspect

T_{TS} = TSI

T_M = RMI

Table 4.2 Prior probabilities for each classified image (%).

Land Cover Class	Prior Probability (1985)	Prior Probability (1992)	Prior Probability (2001)	Prior Probability (2008)
HG	60.3	59.6	57.6	50.4
DSH	8.5	7.6	10.1	9.5
RCK	31.2	32.8	32.3	40.1

A geographic information system union operator was utilized to create the necessary layers for calculating the B_{Prob} . The classified topographic vector layers were input to the union operator. This operator overlays the layers to create a geometric intersection. Polygons output with the same combination of topographic classes were grouped together as multi-part polygons because they shared common topographic characteristics. Multi-part polygons are used to estimate the probability of a land cover class occurring. The area of each unique combination of variables is calculated and used to find the proportion each multi-part polygon had in the entire study area. This procedure is described by Equation 4.3, where:

$$P(T_E \cap T_S \cap T_A \cap T_{TS} \cap T_M) = \frac{A(T_E \cap T_S \cap T_A \cap T_{TS} \cap T_M)}{A_{\text{TOTAL}}}$$

Equation 4.3 Probability of finding unique combinations of topographic variables

Where $A(T_E \cap T_S \cap T_A \cap T_{TS} \cap T_M)$ is the total area of each unique combination of topographic variables and A_{TOTAL} is the total area of the study region. All probability calculations were completed using ArcMap 9.3.

The numerator for Equation 4.1 is calculated in the same manner as Equation 4.3 with the one exception being that the land cover class LC_{ij} is included in the geometric intersection of layers. With these calculations, Equation 4.1 provides the probability of finding a land cover class in a particular year, given the presence of a unique combination of topographic characteristics. The B_{prob} varies over space and are more effective at showing local variation in the probability of being a particular land cover class. Figure 4.12 illustrates areas where DSH was most likely to be found in 2008. The highest values are at the valley bottom and toe slopes where most DSH is found. Probabilities decrease through the transition area with increasing distance away from persistent vegetation. To account for certainty in the B_{prob} land cover values, the classification accuracy, derived from the Kappa Index of Agreement (KIA) were multiplied by the B_{prob} layers for each class. For example, the KIA value for HG in 2008 was 73.4 %, which was multiplied by the B_{prob} layer for HG for the given year. Thus, any pixel in the B_{prob} layer with a value of 1.0, would now have a value of 0.734 or 73.4% (e.g. $1.0 \times 0.734 \times 100$). This reduces the probability of HG occurring at a given pixel, but accounts for uncertainty in the analysis.

The profile plot shown in Figure 4.13 demonstrates how the B_{prob} can vary over space. The profile was digitized in a southwest to northeast orientation from the valley bottom to the higher elevation areas. It shows how the B_{prob} clearly identify the most

favourable areas to find DSH, HG and RCK. There is also evidence that the transition areas between these classes are suitable for more than one class. This indicates there is potential for DSH to move into up-slope areas that are currently only suitable for HG growth.

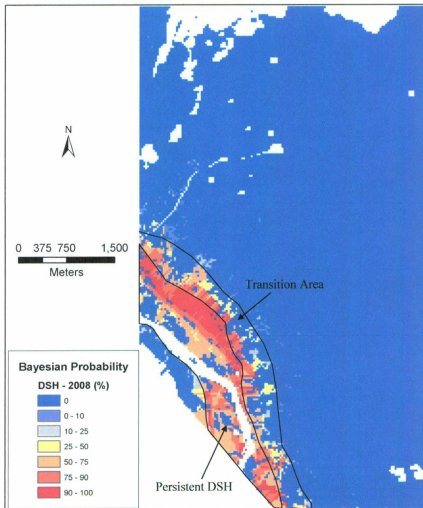


Figure 4.12 Bayesian probability map for DSH in 2008.

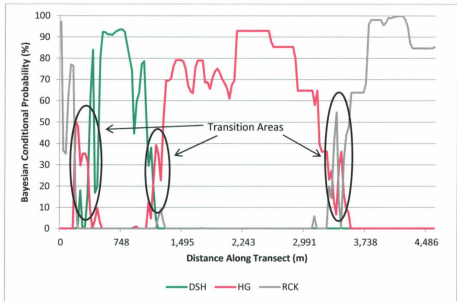


Figure 4.13 Profile of Bayesian conditional probabilities (%).

One B_{Prob} map is generated for each land cover class for each classified image. The change detection analysis using B_{Prob} is discussed in the next section while the integration of B_{Prob} layers in CA-Markov modelling is discussed in Chapter 5.

4.2.2 Bayesian probabilities for change detection

Image differencing techniques are utilized to evaluate the amount of change in B_{Prob} between 1985 and 2008. The B_{Prob} for like classes are subtracted from one another to assess whether the probability of finding a land cover class has increased or decreased over time. The method for determining the difference between images is represented by Equation 4.4 (Nelson, 1983; Singh, 1989).

$$Dx_{ij} = x_{ij}(t_2) - x_{ij}(t_1) \quad \text{Equation 4.4 Image differencing}$$

Where x_{ij} is the pixel value at row i , column j at time (t_1) and (t_2) and Dx_{ij} is the difference at row i , and column j .

Image differencing was performed using a raster data format. The earliest 1985 B_{Prob} layers are subtracted from the 2008 layers to find areas of increase and decrease. To account for certainty in the B_{Prob} the product of the per class KIA values for 1985 and 2008 is multiplied by the resulting change image. This accounted for the error inherent in the classifications. As a result the change image for DSH was multiplied by 1.0, HG was multiplied by 0.428 and RCK by 0.611. The outputs from this analysis are shown in Figures 4.14 through 4.16 respectively.

The percent change in B_{Prob} for DSH (Figure 4.14), ranges from -100% to +100% because the per-class accuracy for the two B_{Prob} layers was 100%. Figure 4.14 shows the overall trend of increasing probability of finding DSH. The general area of persistent DSH (see Figure 4.6) has smaller increases in B_{Prob} values because the vegetation is already well established. Areas along the edge of persistent vegetation are where the largest increases are found. The areas of dark red represent large increases in probability

and visual comparison with Figure 4.6 shows that areas of gain in DSH correspond well with large changes in B_{prob} . There are very few areas of loss for DSH. The most notable area of loss is near the centre of the image which has already been identified as a site of potential misclassification in the 1985 image (Figure 3.6). This map suggests that there is a decrease in the probability of finding DSH at that location.

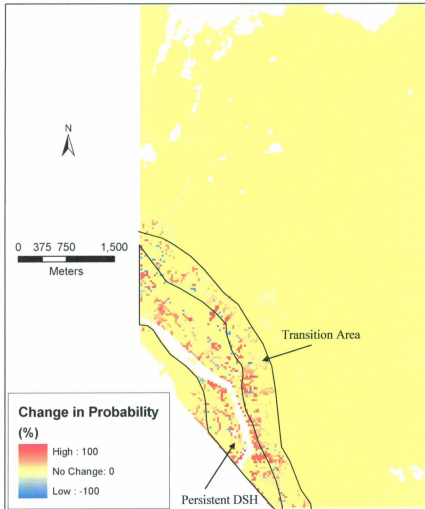


Figure 4.14 Difference in Bayesian probabilities for deciduous shrub between 1985 and 2008.

Figure 4.15 shows the change in B_{Prob} for HG. The majority of change occurs throughout the centre of the study area because this is where HG is primarily located. Most of these areas of change are shaded light blue to represent a decrease in the probability of finding HG. This is in agreement with post classification change comparison discussed earlier, suggesting that HG experienced a loss in area during the past twenty-three years. Figure 4.15 shows that there is a lower probability of finding HG in 2008 than in the past. The increases that were observed tend to have high probabilities, however these areas are very small compared to the areas of loss. The range of increases or decreases is limited to a maximum value of +/- 42.8% because of the accuracy adjustment.

Changes in the RCK class are displayed in Figure 4.16. The post-classification analysis showed that rock was increasing in area over the time series which is consistent with the change in probabilities of finding RCK. Increases in probability occur at higher elevations toward the eastern side of the study area. This area represents the elevational limit of the HG class. These are the types of areas where RCK and HG coexist and the spectral signature of RCK becomes the dominant signature. It is also possible that HG cannot sustain itself in these particular areas, and as a result rock and bare ground has become visible and is being detected by the satellite sensors.

The Bayesian probabilities provide another method of assessing where changes occurred in the landscape and also provide insight into the likelihood of change occurring. If there is historical evidence of change in an area, one can infer these are also potential areas of future change.

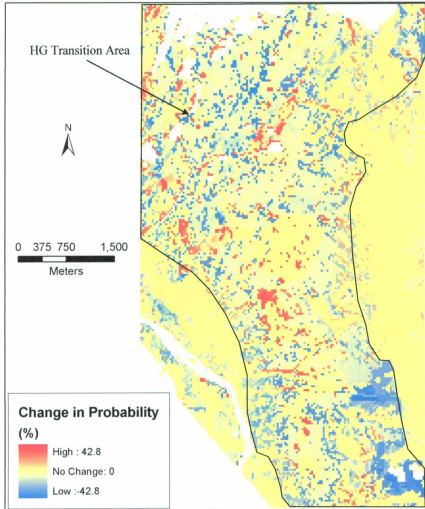


Figure 4.15 Difference in Bayesian probabilities for HG between 1985 and 2008.

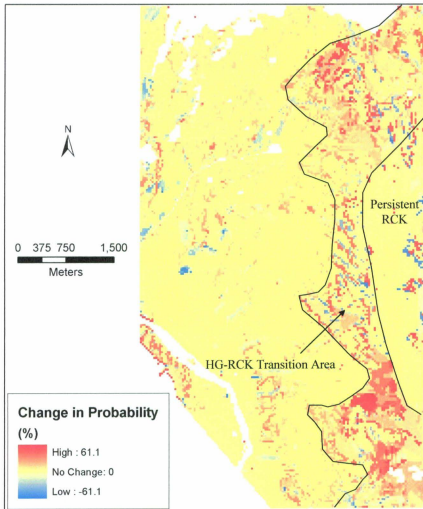


Figure 4.16 Difference in Bayesian probabilities for rock between 1985 and 2008.

The spatial nature of B_{Prob} layers allows for integration into a spatial model. B_{Prob} layers are suitability maps that describe the likelihood of occurrence of a particular land cover. This aspect of the B_{Prob} layers is discussed in Chapter 5 on the development of the CA-Markov model.

4.2.3 Summary of Bayesian Analysis

For each classified image, B_{Prob} layers are calculated for each land cover class. Certainty in the B_{Prob} values was accounted for by multiplying the B_{Prob} layers by per-class KIA values, which were derived from the classified images. B_{Prob} layers were used to determine whether the probability of finding a particular class was increasing or decreasing over time. The analysis revealed that DSH had an increase in the probability of being observed for most locations, whereas HG experienced an overall decrease. Although the loss of HG is due to classification accuracy, these results are in agreement with the post-classification image comparison.

5. Cellular Automata-Markov Chain Modelling Results

5.1 Overview

The CA-Markov model was implemented using a set of modules specifically designed for spatial modelling (Eastman, 2009). An overview of the modelling process is provided here followed by a discussion on error assessment and the procedure of generating predictive models for the study area. Results of the CA-Markov simulations are also presented. Model accuracy is evaluated by comparing the simulated layer and the classification for 2008 as well as assessing the Kappa statistics and cross-classification tables. Matrices generated by the Markov analysis are evaluated and the final simulations from the CA-Markov model are presented.

5.1.1 CA-Markov Model

The spatial modelling modules, available in *Idrisi Taiga*, are specifically designed to run CA-Markov models using classified satellite imagery. A Markovian transition estimator is used to generate transition probability and transition area matrices using a pair of land cover images from different dates. Probability matrices provide the likelihood that a pixel will remain in the same class or transition to another class during the next time period. Transition areas matrices report the expected total area for each vegetation class in the next time period. The module also produced a set of conditional probability images that assign an entire land class a probability of changing to another class. The B_{Prob} values vary within each class and thus provide empirical evidence for the CA model. B_{Prob} layers are used as suitability layers for the remainder of the analysis instead of the Markovian conditional probabilities because of this variation. The number of years between images

must be specified in the model along with the number of years to project into the future. This is used to evaluate changes for discrete time steps and limit the amount of change that can occur in projections. The transition areas matrix was the only result used as direct input into the cellular automata component of the model. The probabilities matrix was used for comparative purposes to test whether or not the transition probabilities become stationary.

The second module required for the analysis combined the stochastic component of the Markov chain with the spatial component of a cellular automata model. To run the CA-Markov model, the most recent classification was input as the base land cover image. This corresponds to the most recent land cover image used in the Markov model. In addition to the image, the Markov model-derived transition areas file was input to define the expected amount of change between classes for a given time period. The transition areas are used to limit the amount of change between classes. This ensures that the projected change is consistent with the amount of observed change and the B_{Prob} layers help determine where the changes will be located. The Bayesian conditional probabilities were used as the input suitability maps for the land cover classes in the model. A 3-by-3 mode filter was applied to each of the B_{Prob} layers to reduce noise and eliminate anomalies that were observed in the preliminary CA-Markov model outputs. To account for certainty in the image classifications, per-class KIA values were multiplied by the B_{Prob} layers used in the analysis. Per-class KIA values can be reviewed in Table 3.9 (Page 46). The B_{Prob} layers represent suitable areas where each land cover can grow because they are based on previously known locations of the vegetation and their preferred topographic conditions. The suitability maps from the Markov model have a single

probability assigned to all cells corresponding to a particular class. The B_{ProbS} have more spatial variation than the Markov derived probabilities. The topographic variables play a crucial role in helping predict land cover distribution. The unique combinations of topographic variables create distinct polygons that are different from its neighbours.

The CA-Markov model outputs a prediction for a specified year using the above input data and a defined neighbourhood. A-3 by-3 Moore neighbourhood was used because it is assumed that the vegetation growth occurs near already persistent areas of that particular vegetation. Field observations and classification maps indicate that the land cover classes are distinct from one another. There is little mixing between HG and DSH as both types have specific areas where they flourish. Additionally, the observed changes in DSH imply that change is occurring within 30 m to 90 m of persistent DSH neighbourhoods. This suggests a 3-by-3 pixel filter (representing an area of 8100m^2) will define the area of vegetation change for this specific study site. The neighbourhood is passed over a Boolean image of each land cover class from the base classification. Pixels falling entirely within the class in question are given a value of one while areas outside are given a value of zero. When the neighbourhood is passed over the border of two different classes the pixels are given values between 0 and 1. This adjusts for the fact that pixels further from the persistent land cover are less likely to change to that class. The result is then multiplied by the suitability map to down-weight the probabilities (Eastman, 2009). The CA-Markov model output is a classified layer that can be compared with classified satellite imagery. The error assessment and specific model runs are discussed in the following sections.

5.1.2 Error Assessment

One convenient method of error assessment in spatial modelling is conducted by predicting the land cover for a time when real conditions are known. This method has been used in other studies such as Araya and Cabral (2010) who used it to verify the accuracy of a model predicting land use change. They predicted the land cover for 2006 using observed changes between 1990 and 2000 images. The simulated 2006 image was then compared to a classified 2006 image using Kappa variation statistics and a cross classification between the two images. The same method was utilized in this study using the 1985 and 2001 classifications to predict the 2008 land cover.

The KIA values are used to compare the known classification to the simulated map. Kappa represents the proportional accuracy adjusted for chance agreement and is subdivided into a variety of components that provide a suitable method for comparing classified imagery (Pontius Jr., 2000). The kappa statistics assess the model accuracy in terms of the quantity of cells properly classified along with the location of the cells. The Kappa statistics, K_{standard} , K_{no} , K_{location} , are summarized in Table 5.1 and described in detail in Pontius Jr. (2000). For this project, the simulated 2008 layer was compared to the classified layer for the same year.

Another method used to assess accuracy is to generate a cross-classification table between the simulated and classified layers for 2008. This table is used to assess the amount of each land cover that was correctly predicted. It also indicates how the simulated layer misclassified pixels. These two methods are good indicators of the effectiveness of the CA-Markov model used in this analysis.

Table 5.1 Description of Kappa statistics for assessing the accuracy of simulated land cover layers (Pontius Jr., 2000).

Kappa Statistic	Description
K_{standard}	A measure of the simulated layers' ability to attain perfect classification.
K_{no}	The proportion of pixels classified correctly relative to the expected proportion classified correctly with no ability to specify quantity or location.
K_{location}	Locational accuracy of pixels in the simulation. Ranges from 0 (random location) to 1 (perfect location specification).

5.2 CA-Markov model development and Accuracy Assessment

The Markovian transition estimator is used to calculate the transition area and probability matrices between 1985 and 2008 classifications. This allows for twenty-three years over which change is detected. Given that vegetation change occurs over a decadal time scale, ten year increments are used for the simulations. Projections are made for 2018, 2028 and 2038. The CA-Markov model assumes the changes that have occurred are likely to be repeated over the same time period but beyond that, the transitions are unknown. For this reason only one projection beyond the temporal range of the data was used.

The cellular automata model incorporated the transition area files from the Markov analysis as well as the Bayesian conditional probability dataset to formulate the hybrid CA-Markov model. Bayesian conditional probability data, corresponding to 2008, is used for each simulation because it provides the most accurate representation of suitable areas of vegetation growth. The model produced three land cover maps that are analyzed using post-classification image comparison. Changes are quantified and

compared to known changes to assess whether the model accurately represented future conditions.

As a model indication process, the CA-Markov model was used to predict the 2008 land cover classification. Figure 5.1 shows both the original 2008 classification and the simulated layer. Visually, the most notable difference is the actual classification had more spatial variability throughout each land cover. This is particularly evident in the HG dominated area where there is a lot of mixing with the RCK class (Figure 5.1). The simulated layer has a smoother, more continuous appearance. This is because of the 1985 (Figure 3.6, P. 40) and 2001 (Figure 3.10, P. 49) classifications have a more continuous appearance than the 2008 classification. Since the simulation is based on those images, it maintains those characteristics. Aside from this difference, the simulated layer retains the overall pattern of vegetation throughout all three classes.

The K_{no} value is a better alternative than $K_{standard}$ for assessing the overall accuracy of the model (Pontius Jr., 2000). At 70.8%, the 2008 model performed well in its overall ability to predict land cover. Models with accuracies in excess of 80% are typically considered very strong predictive tools (Araya and Cabral, 2010). Guisan and Zimmermann (2000) suggest that any model with a K value greater than 0.5 is considered fair. This is considered an effective method of modelling the landscape as it is within this accepted range. The $K_{location}$ value of 75.6% indicates that the model provides a reasonable representation of location and based on the Kappa values the model will reliably predict future land cover conditions. A cross-classification table was used to

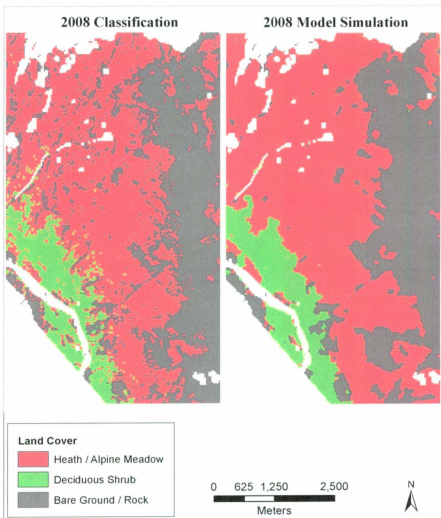


Figure 5.1 Original 2008 classification (left) and the simulated 2008 classification (right).

assess the accuracy of the 2008 simulation. Table 5.2 shows the counts of pixels that are classified the same on both the classification and the model. The simulation predicted the 2008 land cover with an overall Kappa value of 66%. Per-class KIA values for HG (71.4%) and DSH (86.7%) suggest that those classes were predicted dependably in the model (Table 5.2). RCK had a much lower KIA value at 55.1% which could be caused by pixel mixing with the HG class. Table 5.2 shows that 3760 pixels were simulated as being HG when they should have been RCK. This implies that the model does not predict RCK as well as the vegetation classes.

Table 5.2 Cross-classification table for the original 2008 classification and the 2008 simulation.

		Classification			
		HG	DSH	RCK	KIA Value (%)
Simulation	HG	14417	321	3760	71.4
	DSH	531	2748	197	86.7
	RCK	1517	50	9167	55.1

5.3 Transition Matrices

Transition matrices generated by the Markov model provide information about the amount of change and likelihood of change occurring before the final CA-Markov model was produced. This section discusses the matrices for the three projections to show how each land cover was projected to change. Transition area matrices were compared to the total known areas of land derived from the classifications. The transition probability matrix provides an initial indication of how the likelihood of belonging to a particular class, changes over time. Each of these is discussed in more detail below.

5.3.1 Transition Area Matrices

Transition area matrices are used to assess the amount of area expected to change between land cover classes for the different simulations. The three transition areas matrices are displayed in Tables 5.3 to 5.5. Of particular interest is the relationship between HG and DSH and, to a lesser extent, the relationship between HG and RCK. Each matrix shows that the transition from HG to DSH is always greater than the amount of change from DSH to HG. This results in a very small net gain for the DSH class. Along with the small increase in DSH from RCK, this means that the DSH class should experience small gains in total area.

The losses of HG to DSH and RCK far outweigh the gains in HG. This implies that HG should experience a net loss in area. Much of the loss in HG resulted in an increase of RCK because it would have been exposed as the vegetation retreated. These transition area matrices show that the Markov component of the model effectively predicts proportions of each land cover class. The total percent cover of DSH and RCK increase with longer projections. The total percent cover for HG decreases over the time series of projections. This is consistent with change detection analysis where it was observed that DSH and RCK increased in total area by 10.7% and 22.2% respectively and HG decreased by 19.7%.

Table 5.3 Transition area matrix for the 2018 projection (%).

		To (2018)		
		HG (%)	DSH (%)	RCK (%)
From (2008)	HG	42.7	1.05	6.61
	DSH	0.85	8.68	0
	RCK	3.44	0.12	36.56
	Total	46.99	9.85	43.17

Table 5.4 Transition area matrix for the 2028 projection (%).

		To (2028)		
		HG (%)	DSH (%)	RCK (%)
From (2008)	HG	38.06	1.73	10.54
	DSH	1.55	7.98	0
	RCK	5.53	0.33	34.26
	Total	45.14	10.04	44.80

Table 5.5 Transition area matrix for the 2038 projection (%).

		To (2038)		
		HG (%)	DSH (%)	RCK (%)
From (2008)	HG	33.29	2.42	14.67
	DSH	2.15	7.31	0
	RCK	7.71	0.52	31.93
	Total	43.15	10.25	46.60

5.3.2 Transition Probability Matrices

The transition probability matrices give the likelihood of transition between classes. The matrices presented in Tables 5.6 to 5.8 give the likelihood a particular class from 2008, will change to another class or remain the same in the future. One trend is that over the three projections the probability of remaining in the same class decreases. HG experiences the biggest drop between the first and last projections. After ten years, there is an 84.7% chance a current HG pixel will still be HG however after thirty years that value drops to 66.1%. It is also more likely for the HG class to transition to RCK rather than DSH which is shown throughout Tables 5.6 to 5.8. There is a 29.1% chance that a pixel representing HG in 2008, has turned to RCK by 2038. Other notable trends show that the current DSH class is only going to turn into HG while RCK is more likely to change to HG.

These matrices establish that the Markov chain assessed the changes between the classified imagery for 1985 and 2008 and dependably based the projected probability of change on observed values. The Markov model provided a suitable output for the cellular automata component in terms of the area matrices. The results of the CA-Markov model are discussed in the following section.

Table 5.6 Transition probability matrix for the 2018 projection

		Probability of Changing To (%) (2018)		
		HG	DSH	RCK
From (2008)	HG	84.7	2.1	13.1
	DSH	8.9	91.0	0
	RCK	8.6	0.3	91.1

Table 5.7 Transition probability matrix for the 2028 projection

		Probability of Changing To (%) (2028)		
		HG	DSH	RCK
From (2008)	HG	75.6	3.4	20.9
	DSH	16.3	83.7	0
	RCK	13.8	0.8	85.4

Table 5.8 Transition probability matrix for the 2038 projection

		Probability of Changing To (%) (2038)		
		HG	DSH	RCK
From (2008)	HG	66.1	4.8	29.1
	DSH	22.6	76.6	0.8
	RCK	19.2	1.3	79.5

5.4 Cellular Automata-Markov Chain Simulations

The results of the CA-Markov model for 2018, 2028, and 2038 are presented in this section. Figure 5.2 represents the three projected land cover maps generated using the CA-Markov approach. Each land cover does not exhibit dramatic changes at any point throughout the time series. As a result, the projections maintain the gradual transition that was observed between 1985 and 2008. The changes in distribution were quantified in terms of change in area.

Each land cover class exhibited the same trend in change that was observed from the classified imagery. Figure 5.3 illustrates that HG continued to decline in total area while RCK increased in total area. The DSH region remained relatively constant compared to the other two classes so it can be assumed that loss of HG contributed to the majority of gain in RCK. Figure 5.4 illustrates DSH increased in area by 0.14 km^2 between 2008 and the 2038 projection which accounts for a 7.7% increase in total areal coverage of DSH. This is slightly smaller than the 10.8% increase observed between 1985 and 2008. The changes for HG and RCK are also lower for the projection than the actual observed change. Figure 5.5 shows that the model consistently underestimates the amount of change in area compared to what was observed. The B_{prob} suitability layers can cause underestimation if there are no suitable areas for change to occur. Thus the topographic variables are acting as a constraint because the combinations of variables define areas where vegetation is likely to grow. This is a limitation of the environment and the available suitable habitat in the study area. B_{prob} will have low probability at sites where there is no evidence of past vegetation growth, therefore the model will not predict vegetation growth at those sites.

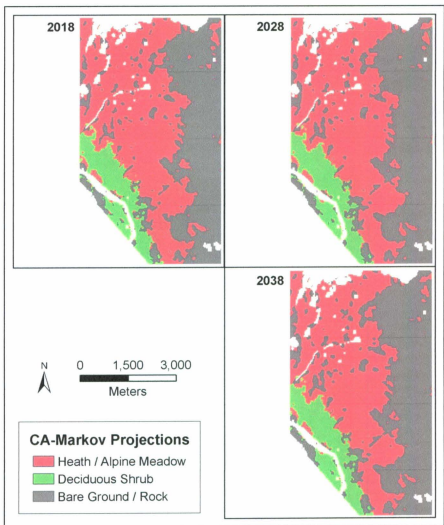


Figure 5.2 Projected land cover distributions using CA-Markov chain model.

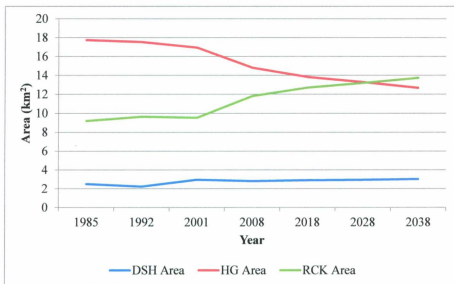


Figure 5.3 Area of each land cover class as represented by the classified imagery and model projections.

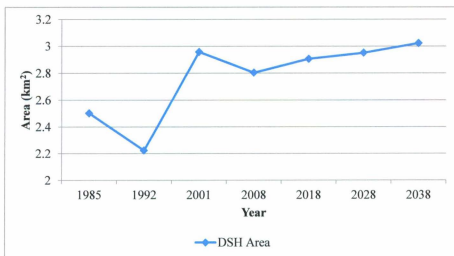


Figure 5.4 Area of DSH from the classified imagery and the model projections

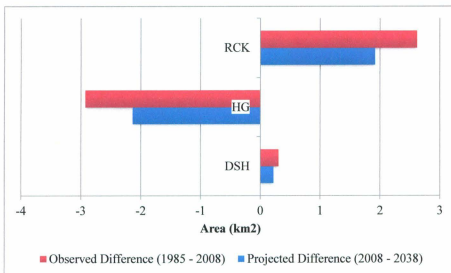


Figure 5.5 Differences in area as observed from classified imagery and projected by the CA-Markov model.

Change maps generated for the 2038 projection show where land cover changes are most likely to occur. Figure 5.6 displays the transitions between all classes for the 2038 projection. HG to RCK is the most dominant transition observed in the projected land cover. Most of that change occurred on the eastern side of the study area, which corresponds with mid to high elevations. This is where HG transitions into RCK and is the expected area of change for these classes. Figure 5.7 displays the area where HG was lost to RCK thus giving a better perspective of the projected change. It shows that HG is decreasing along the boundary with RCK. This suggests that any change in vegetation cover will occur along the edges of persistent vegetation.

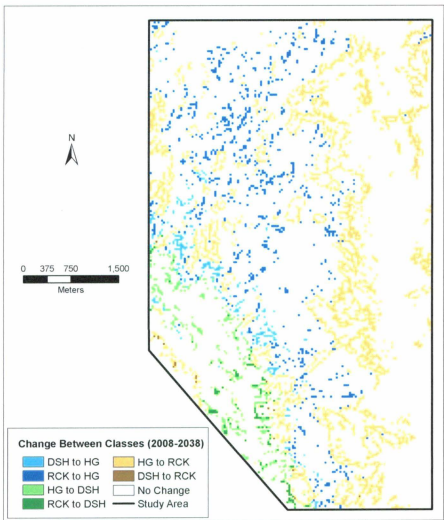


Figure 5.6 Transitions between classes for the 2038 CA-Markov projection.

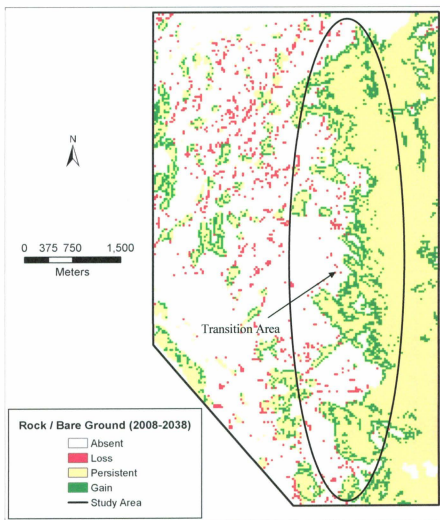


Figure 5.7 Gains and losses in RCK for the 2038 CA-Markov chain projection

The model accurately depicts where changes are expected to occur; this is in agreement with the observed changes in RCK land cover. Losses in RCK occur primarily in the centre part of the study area. This coincides with persistent areas of HG. Figure 5.6 shows that both DSH and RCK contribute to gains in HG. Figure 5.8 shows that losses in area of HG are much more dominant than the gains. This agrees with the observations between 1985 and 2008 that showed net losses in the HG class. Also, much of this loss occurred along the boundary with adjacent classes and therefore it is occurring in areas where change is expected. A loss in HG is not the normal transition one would expect. This transition is related to classification error in the RCK and HG classes.

Gains and losses in the DSH class are concentrated in the southwest portion of the study region which indicates that the model is accurately predicting the best potential locations for vegetation growth. Figure 5.9 displays the areas of gains and losses in DSH while Figure 5.6 shows that the majority of gains come from the HG class with only a small contribution from RCK. Gains occurred mostly along the eastern edge of persistent DSH and infilling was indicated by increasing B_{Prob} values. The losses occurred among more dispersed regions of DSH. Small clusters of DSH located away from the large persistent region were the areas that transitioned to another vegetation class in the model.

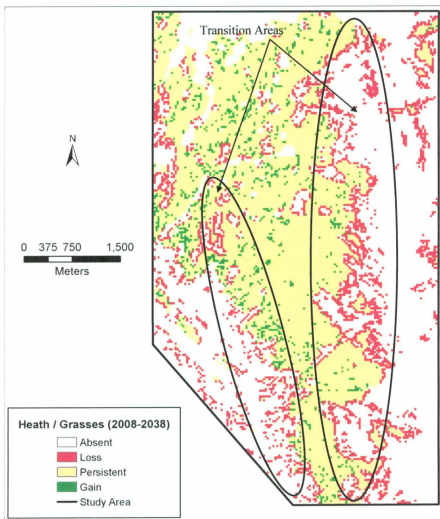


Figure 5.8 Gains and losses in HG for the 2038 CA Markov projection

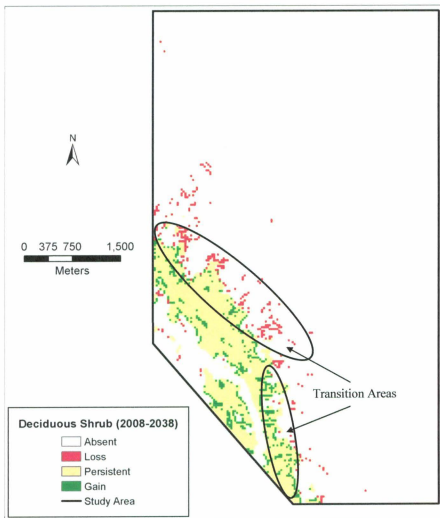


Figure 5.9 Gains and losses in DSH for the 2038 CA-Markov projection

The model appears to accurately represent future land cover based on the amount of change that was detected. It correctly projected small gains in the DSH land cover and large gains in RCK. It also effectively showed the losses in HG and established that most of the transition in the landscape is between the HG and RCK classes. The Markov component of the model is responsible for this because it restricted the amount of change that occurred between classes based on past change.

The cellular automata component of the model also correctly positioned the changes for each land cover. This was limited by the defined Moore neighbourhood, as well as the Bayesian conditional probabilities which helped define suitable areas of growth for each land cover and introduced uncertainty into the model.

One particular tendency of the model was that it generated smoother, more continuous surface classes. The classes in each of the projections (Figure 5.2) were more continuous than the 2008 classification (Figure 3.11, P. 50). This is partly because the model identified small regions entirely surrounded by a particular class to be the most suitable to transition into that class. The resulting projections are visually more similar to the classifications developed for the Landsat imagery for 1985, 1992, and 2001.

5.5 Summary of Results

The CA-Markov model was used to predict 2008 land cover conditions as a measure of model accuracy. The K_{60} value of 70.8% suggests that the model reasonably predicts current land cover conditions. Per-class, Kappa index of agreement (KIA) statistics were also calculated as local measures of accuracy whereby HG (71.4%) and DSH (86.7%) are well classified. RCK (55.1%) was poorly classified because of mixing with the HG class.

Transition probability matrices assessed the likelihood of change occurring between classes. These results suggest that by 2038, 33.9% of HG will have transitioned to DSH (4.8%) or RCK (29.1%). Shrub and rock are projected to gain in total area over that time frame. The CA-Markov simulations are consistent with the observed patterns of change and show that DSH and RCK will continue to expand in the future while HG will experience a decrease in total area. The model also shows that gains and losses of each class occur along transition areas between land covers. The amount of projected change is less than what was observed between 1985 and 2008 for each of the land classes but the locations of the changes are consistent with observations from historic satellite data.

6. CONCLUSION

The primary objective of this study was to develop a CA-Markov model to predict future vegetation patterns based on topographic conditions and observed changes in land cover.

In order to achieve this objective, four sub-objectives were completed:

1. A time series of classified satellite imagery was created.
2. Change detection methods were used to determine the amount of vegetation change over the time series, and where it occurred in the landscape.
3. A set of suitability maps were created using Bayesian probability methods.
4. A CA-Markov model was generated that effectively predicted current vegetation distribution, based on historical evidence.

6.1 Classified Time Series

Landsat images were obtained for 1985, 1992 and 2001 along with a SPOT image taken in 2008. The images were taken between late July and late August to minimize seasonal variation in vegetation growth. Images were pre-processed and resampled to 30 m resolution to comply with IPY CiCAT protocol (Chen, *et al.*, 2007). A maximum likelihood supervised classification was used to classify each image into three distinct land cover classes. Heath/grass (HG), deciduous shrub (DSH), and rock (RCK) were established as three classes that could be effectively distinguished from one another at the 30 m resolution. This classification scheme achieved high accuracy rates for the classified imagery. The lowest accuracy was for 1985 but this was expected because 2008 field data was used to classify all images. Lower classification accuracy for 1985 might be an indication of vegetation change over the temporal span of the data. The land cover maps provided input for change detection analysis and the CA-Markov model.

6.2 Change Detection Analysis

Change detection analysis quantified the amount of change between classified images and provided methods to assess the changes between the different classes. DSH and RCK experienced an increase in areal extent of 10.7% and 22.2% respectively. These gains came at the expense of HG which experienced a decrease of 19.7% over the twenty-three years. A decrease in HG is not commonly found in other studies of alpine vegetation. The decrease observed here is likely due to low classification accuracies of the 1985 satellite image.

Mapping the distribution of the changes showed that most gains and losses in total area for a given land cover occur along the boundaries of the persistent land cover class. This suggests that a cellular automata method of modelling is effective because neighbourhood and suitability maps define potential areas of growth. It was also shown through change detection analysis that the change was a continuous process, thus the greatest amounts of change are observed over the twenty-three year time series. The model was implemented using ten year intervals up to thirty years past the most recent satellite imagery.

6.3 Bayesian Probabilities

Bayesian conditional probabilities were used to define suitable areas for each land cover class and were based on the unique combinations of topographic variables. The highest conditional probabilities for any class are located in the areas where a particular land cover is present. B_{Prob} values decreased with increasing distance away from the present

land cover conditions. The B_{Prob} layers provide suitability map inputs for the CA-Markov model.

The layers were also used as an alternative method of change detection. Image differencing methods are used on the probability maps for different years. The output identified areas where the probability of finding a particular land cover class had increased and decreased over time. Increasing probabilities represent areas where vegetation was becoming denser and well established in the landscape. Decreasing probabilities represent areas where a land cover class is being overtaken by a different land cover class. This change analysis is an alternative method of looking at how the classes are changing within the landscape. These results are consistent with the post-classification image comparison.

6.4 CA-Markov Model Accuracy Assessment

To assess the accuracy of the CA-Markov model for this research, a predicted classification was made for a time period during which a known classification was available (Araya and Cabral, 2010). Using Kappa statistics, the predicted and observed classifications were compared. The validation model predicted the 2008 land cover with 70.8% accuracy. HG and DSH had the best classification accuracies at 71.4% and 86.7% respectively. The model maintained the general structure of the land cover classes as well as the observed pattern. The DSH class dominated the southwest part of the study area, while RCK was located primarily to the east and HG was located between the two classes, at mid elevations. One noticeable feature of the output model is that it generated smoother, more continuous groups of pixels for each class. The classified 2008 image is

very fragmented with small clusters of pixels representing one class, being mixed with another class. This is generally absent from the projections and is a result of the neighbourhood used in the CA-Markov model. All of those small clusters of pixels are identified as places that have a high probability of changing to the dominant class in the area. These small areas are amongst the first to change in the simulation. Given the results, this model could be used to make future predictions concerning land cover distribution in the Torngat Mountains but it could be improved with some additions to the modelling process.

A more extensive vegetation survey coupled with higher resolution satellite imagery would greatly improve image classification for the region. Higher classification accuracy would lead to greater certainty in modelling results. Further research into what topographic variables affect tundra vegetation would also help refine the Bayesian probabilities. The most important topographic variables relating to vegetation habitat have not yet been identified for the study area. Understanding what those variables are would result in better suitability maps on which the CA-Markov model is based.

6.5 Modelling Future Land Cover Scenarios

The four sub-objectives of the research generated the information and data required to use a CA-Markov chain model to simulate future land cover scenarios in the Torngat Mountains. The time series of satellite imagery is the most important information for the research. High accuracy rates for the DSH class allowed for more certainty in the final outputs. Change detection analysis results showed that change in vegetation patterns occurred at the study area between 1985 and 2008. This suggests that there is a dynamic

process at work and it provided a baseline for which future projections of change was compared. Bayesian probabilities provided an alternative set of suitability maps that incorporated site specific information into the model. The probability layers provided a better representation of suitable areas of vegetation growth because it incorporated information on preferred growing conditions based on the topographic variables. Finally, the accuracy assessment of the model demonstrated that the CA-Markov chain method is an effective method of modelling future vegetation patterns for the study area.

The CA-Markov model was implemented using the 2008 classified image as the base land cover and the Bayesian conditional probabilities for 2008 as the suitability maps. Outputs for the three projected years gave consistent trends compared to the amount of change that was observed between 1985 and 2008. The HG class continued to lose area while RCK and DSH experienced increases in area. The model also appropriately located the most likely areas for change to occur. The projections showed that gains in DSH were primarily located along the edges of the persistent land cover. This implies that the shrubs will grow outward from existing vegetation into adjacent areas if the topographic conditions are suitable. Similarly, losses in HG and gains in RCK occur mainly along the boundary between those two classes.

The predicted land cover scenarios suggest that relatively small amounts of change will occur amongst the DSH class. Shrubs accounted for 9.5% of the total area in 2008 and were projected to occupy 10.3% in 2038. That is a 7.7% increase in the total area of DSH over a 30 year period. The model predicts that DSH will move tens of meters upslope over the next thirty years. This limited movement is not enough to suggest that DSH will be able to move into higher elevations and become the dominant vegetation in

the study area. RCK, on the other hand increased from 40.1% to 46.7% total coverage. That amounts to a 16.2% increase in total area. HG dropped from 50.3% to 43.1%, a loss of 14.4% in heath. Although the change detection analysis and projections from the model show HG is losing a lot of area to RCK, it is still the dominant land cover at mid-elevations. Previous studies have documented that some species are intolerant to competition and therefore have decreased in abundance with the onset of warming and greater nutrient availability (Gottfried *et al.*, 1999; Jagerbrand *et al.*, 2009; Pauli *et al.*, 2007). These situations imply that certain species or functional groups are being replaced by other vegetation. The results here show that the HG is retreating and leaving rock and bare ground exposed. This does not suggest competition is an issue because the HG is not being replaced by other types of vegetation. One potential cause of the loss of HG could be related to frost damage. Increased occurrences of intense cooling, followed by warming periods during the spring green-up will make vegetation more susceptible to damage during these events. If the intense cooling periods increase in frequency than there is a possibility that the vegetation could die and show a pattern of retreat. This is possible in the Torngat Mountains where there is less snow cover and vegetation is exposed earlier in the season. The vegetation in these areas could potentially retreat if these events occur repeatedly over multiple years. Gu, *et al.* (2008) looked at a spring freeze event in the United States and found considerable frost damage that devastated crops in the southern United States.

This issue might also be related to classification issues. HG and RCK are known to co-exist in the landscape, thus RCK might have more dominant reflectance in these areas. Further refinement of the classification is necessary to identify and correct these

issues, if they exist. A more extensive vegetation survey would be required to target those areas and see what is causing this perceived vegetation retreat.

6.6 Implications

Assuming that the predictions resulting from this research will occur over the next thirty years, it appears that there is little threat of deciduous shrubs encroaching on existent heathlands in this area of the Torngat Mountains. The movement that was observed and predicted shows that it may take centuries for shrubs to dominate the landscape at higher elevations and will never exist in more exposed, rocky areas. Aspect and slope will not restrict the growth of DSH in the study site and elevation will not limit growth given the current position of vegetation. The biggest habitat constraint will likely be the presence or absence of RCK. The higher elevations and absence of soil in areas of RCK will prevent DSH from growing in those areas. Interactions between the HG and RCK must be further analyzed to assess the present state of HG. Future studies involving remotely sensed image analysis should incorporate higher resolution imagery if it is available, along with more extensive field analysis. This would provide a better indication of the state of heath in the Torngat Mountains.

7. References

- ACIA. (2005). *Arctic Climate Impact Assessment*. Cambridge University Press.
- Araya, Y. H., and Cabral, P. (2010). Analysis and modeling of urban land cover change in Setubal and Sesimbra, Portugal. *Remote Sensing*, 2, 1549 - 1563.
- Aspinall, R. (1992). An inductive modelling procedure based on Bayes' theorem for analysis of pattern in spatial data. *International Journal of Geographical Information Systems*, 6(2), 105-121.
- Babish, G. (2006). *Geostatistics Without Tears*. Environment Canada, Ecological Research Division, Regina.
- Balzter, H. (2000). Markov chain models for vegetation dynamics. *Ecological Modelling*, 126, 139-154.
- Balzter, H., Braun, P. W., and Kohler, W. (1998). Cellular automaton models for vegetation dynamics. *Ecological Modelling*, 107, 113-125.
- Benabdellah, B., Albrecht, K.-F., Pomaz, V. L., Denisenko, E. A., and Logofet, D. O. (2003). Markov chain models for forest successions in the Erzgebirge, Germany. *Ecological Modelling*, 159, 145-160.
- Bennie, J., Hill, M. O., Baxter, R., and Huntley, B. (2006). Influence of slope and aspect on long-term vegetation change in British chalk grasslands. *Journal of Ecology*, 94, 355-368.
- Bonham-Carter, G. F. (1994). *Geographic Information Systems for Geoscientists*. New York: Pergamon.
- Bonham-Carter, G. F., Agterberg, F. P., and Wright, D. F. (1988). Integration of geological datasets for gold exploration in Nova Scotia. *Photogrammetric Engineering and Remote Sensing*, 54 (11), 1585-1592.
- Cannone, N., Sgorbati, S., and Guglielmin, M. (2007). Unexpected impacts of climate change on alpine vegetation. *Frontiers in Ecology and the Environment*, 5 (7), 360-364.
- Chavez Jr., P. S. (1996). Image based atmospheric corrections - Revisited and improved. *Photogrammetric Engineering and Remote Sensing*, 62 (9), 1025-1036.

- Chen, W., Armenakis, C., Blain, D., Brook, R., Cyr, I., McDonald, K., Dyke, L., Fernandes, R., Fraser, R., Grieve, S., Hamilton, K., Helie, R., Johnson, V., Kochler, K., Latifovic, R., Leblanc, S., Li, J., McLennan, D., Moghaddam, M., Olthoff, I., Perrott, T., Sladen, W., Valteau, R., Wang, J., Wang, S., Wu, W., Zhang, Yi., Zhang, Yu. (2007). IPY CiCAT Field Measurement Protocol for Mapping Canada's Arctic Vegetation. Version 4.0
- Clark, P. U. (1991). Canadian Landform Examples-20: Landscapes of glacial erosion, Torngat Mountains, Northern Labrador/Ungava. *The Canadian Geographer*, 35 (2), 208-213.
- Clark, P. U. (1988). Glacial geology of the Torngat Mountains, Labrador. *Canadian Journal of Earth Sciences*, 25, 1184-1198.
- Colasanti, R. L., Hunt, R., and Watrud, L. (2007). A simple cellular automaton model for high-level vegetation dynamics. *Ecological Modelling*, 203, 363-374.
- Congalton, R.G. and Mead, R.A. (1983). A quantitative method to test for consistency and correctness in photointerpretation. *Photogrammetric Engineering and Remote Sensing*. 49(1), 69-74.
- De Smith, M. J., Goodchild, M. F., and Longley, P. A. (2007). *Geospatial Analysis: A comprehensive guide to principles, techniques and software tools* (2nd ed.). Leicester, UK: Matador.
- Dobos, E., Daroussin, J., and Montanarella, L. (2005). *An SRTM-based procedure to delineate SOTER Terrain Units on 1:1 and 1:5 million scales*. Luxembourg: Office for Official Publications of the European Communities.
- Eastman, R. (2009). *Idrisi Taiga: Guide to GIS and Image Processing*. Clark University. Worcester: Clark University.
- Eastman, R., Sangermano, F., Ghimire, B., Zhu, H., Chen, H., Neeti, N., Cai, Y., Machado, E., Crema, S. (2009). Seasonal trend analysis of image time series. *International Journal of Remote Sensing*, 30(10), 2721-2726.
- Franklin, J. (1995). Predictive vegetation mapping: geographic modelling of biospatial patterns in relation to environmental gradients. *Progress in Physical Geography*, 19 (4), 474-499.
- Fu, B. J., Liu, S. L., Ma, K. M., and Zhu, Y. G. (2004). Relationships between soil characteristics, topography and plant diversity in a heterogeneous deciduous broad-leaved forest near Beijing, China. *Plant and Soil*, 261, 47-54.
- Gottfried, M., Pauli, H., Reiter, K., and Grabherr, G. (1999). A fine-scaled predictive model for changes in species in species distribution patterns of high mountain plants induced by climate warming. *Diversity and Distributions*, 5 (6), 241-251.

- Gu, L., Hanson, P.J., Post, W.M., Kaiser, D.P., Yang, B., Nemani, R., Pallardy, S.G., Meyers, T. (2008) The 2007 Easter US Spring Freeze: Increased Cold Damage in a Warming World. *Bioscience* 58, 253-262.
- Guisan, A., and Zimmermann, N. E. (2000). Predictive habitat distribution models in ecology. *Ecological Modelling*, 135, 147-186.
- Hall, F.G., Strebel, D.E., Nickeson, J.E., and Goetz, S.J. (1991). Radiometric rectification: Toward a common radiometric response among multitemporal, multisensor images. *Remote Sensing of Environment*, 35, 11-27.
- Henry, G. (2010). *Climate Change Impacts on Canadian Arctic Tundra*. Retrieved 04 15, 2010, from <http://ipy.tundra.ca/>
- Hutchinson, M. F., McKenney, D. W., Lawrence, K., Pedlar, J. H., Hopkinson, R. F., Milewska, E., Papadopol, P. (2009). Development and testing of Canada-wide interpolated spatial models of daily minimum-maximum temperature and precipitation for 1961-2003. *Journal of Applied Meteorology and Climatology*, 48, 725-741.
- Isagi, Y., and Nakagoshi, N. (1990). A Markov approach for describing post-fire succession of vegetation. *Ecological Research*, 5, 163-171.
- Intergovernmental Panel on Climate Change (IPCC) (2007). *Climate Change 2007: The Physical Science Basis*. S. Solomon, M. Qin, M. Manning, Z. Chen, M. Marquis, K. Averyt, M. Tignor and H.L. Miller (eds.) Cambridge, UK: Cambridge University Press.
- Jägerbrand, A. K., Alatalo, J. M., Chrimes, D., and Molau, U. (2009). Plant community responses to 5 years of simulated climate change in meadow and heath ecosystems at a subarctic-alpine site. *Oecologia*, 161, 601-610.
- Jia, G., Epstein, H., and Walker, D. (2009). Vegetation greening in the Canadian arctic related to decadal warming. *Journal of Environmental Monitoring*, 11, 2231-2238.
- Körner, C., and Paulsen, J. (2004). A world-wide study of high altitude treeline temperatures. *Journal of Biogeography*, 31, 713-732.
- Labrador Highlands Research Group. (2010). Retrieved 04 15, 2010, from <http://www.mun.ca/geog/lhrg/>
- Lanzer, A. T., and Pillar, V. D. (2002). Probabilistic cellular automaton: model and application to vegetation dynamics. *Community Ecology*, 3 (2), 159-167.
- Lippe, E., De Smidt, J. T., and Glenn-Lewin, D. C. (1985). Markov models and succession: A test from a heathland in the Netherlands. *The Journal of Ecology*, 73 (3), 775-791.

- Lunetta, R. S. (1998). Applications, Project Formulation, and Analytical Approach. In R. S. Lunetta, and C. D. Elvidge (eds.), *Remote Sensing Change Detection: Environmental Monitoring Methods and Applications* (pp.1-19). Chelsea, Michigan: Ann Arbor Press.
- Mas, J. F. (1999). Monitoring land-cover changes: a comparison of change detection techniques. *International Journal of Remote Sensing*, 20 (1), 139-152.
- McCarthy, M. A. (2007). *Bayesian Methods for Ecology*. Cambridge: Cambridge University Press.
- McNab, H. W. (1989). Terrain shape index: Quantifying effect of minor landforms on tree height. *Forest Science*, 35 (1), 91-104.
- Meades, S. (1990). *Natural Regions of Newfoundland and Labrador*. St. John's: Protected Areas Association.
- Moore, I. D., Grayson, R. B., and Ladson, A. R. (1991). Digital terrain modelling: A review of hydrological, geomorphological, and biological applications. *Hydrological Processes*, 5, 3-30.
- Moore, I., Gessler, P., and Nielsen, G. (1993). Soil attribute prediction using terrain analysis. *Soil Science Society of America Journal*, 57, 443-452.
- Nelson, R. F. (1983). Detecting forest canopy change due to insect activity using Landsat MSS. *Photogrammetric Engineering and Remote Sensing*, 49 (9), 1303-1314.
- Ostendorf, B., and Reynolds, J. F. (1998). A model of arctic tundra vegetation derived from topographic gradients. *Landscape Ecology*, 13, 187-201.
- Pauli, H., Gottfried, M., and Grabherr, G. (1996). Effects of climate change on mountain ecosystems - Upward shifting of alpine plants. *World Resource Review*, 8 (3), 382-390.
- Pauli, H., Gottfried, M., Reiter, K., Klettner, C., and Grabherr, G. (2007). Signals of range expansions and contractions of vascular plants in the high Alps: observations (1994-2004) at the GLORIA master site Schrankogel, Tyrol, Austria. *Global Change Biology*, 13, 147-156.
- Pontius Jr., R. (2000). Quantification error versus location error in comparison of categorical maps. *Photogrammetric Engineering and Remote Sensing*, 66 (8), 1011-1016.
- Pueyo, Y., and Begueria, S. (2007). Modelling the rate of secondary succession after farmland abandonment in a Mediterranean mountain area. *Landscape and Urban Planning*, 83, 245-254.

- Rezaei, S. A., and Gilkes, R. J. (2005). The effects of landscape attributes and plant community on soil physical properties. *Geoderma*, 125, 145-154.
- Rosenfield, G. H., and Fitzpatrick-Lins, K. (1986). A coefficient of agreement as a measure of thematic classification accuracy. *Photogrammetric Engineering and Remote Sensing*, 52 (2), 223-227.
- Rossi, R. E., Dungan, J. L., and Beck, L. R. (1994). Kriging in the shadows: Geostatistical interpolation for remote sensing. *Remote Sensing of the Environment*, 49, 32-40.
- Silvertown, J., Holtier, S., Johnson, J., and Dale, P. (1992). Cellular automaton models of interspecific competition for space - the effect of pattern on process. *Journal of Ecology*, 80, 527-534.
- Singh, A. (1989). Digital change detection techniques using remotely sensed data. *International Journal of Remote Sensing*, 10 (6), 989-1003.
- Usher, M. B. (1981). Modelling ecological succession, with particular reference to Markovian models. *Vegetatio*, 46, 11-18.
- Vaiphasa, C., Skidmore, A. K., and de Boer, W. F. (2006). A post-classifier for mangrove mapping using ecological data. *Photogrammetry and Remote Sensing*, 61, 1-10.
- Van Der Meer, F. (1996). Classification of remotely-sensed imagery using an indicator kriging approach: application to the problem of calcite-dolomite mineral mapping. *International Journal of Remote Sensing*, 17 (6), 1233-1249.
- Weismiller, R. A., Kristof, S. J., Scholz, D. K., Anuta, P. E., and Momin, S. A. (1977). Change detection in coastal zone environments. *Photogrammetric Engineering and Remote Sensing*, 43 (12), 1533-1539.
- Wolfram, S. (1983). Statistical mechanics of cellular automata. *Reviews of Modern Physics*, 55 (3), 601-643.
- Young, J. (2006). *Ecological Land Units of Shenandoah National Park*. Retrieved 06 14, 2009, from United States Geological Survey:
<http://lsc.usgs.gov/gis/shen/shenveg/envirogradients.asp#reclass>
- Yuan, D., Elvidge, C. D., and Lunetta, R. S. (1998). Survey of Multispectral Methods for Land Cover Change Analysis. In R. S. Lunetta, and C. D. Elvidge (eds.), *Remote Sensing Change Detection: Environmental Monitoring Methods and Applications* (pp. 21-39). Chelsea, Michigan: Ann Arbor Press.
- Zimmermann, N. E. (2001). *Topographic Position Mapping Routines*. Retrieved 8 2, 2009, from Tools for analyzing, summarizing, and mapping of biophysical variables:
<http://www.wsl.ch/staff/niklaus.zimmermann/progs.html>

APPENDIX A: FIELD DATA

